Available online at www.sciencedirect.com
ScienceDirect
Journal of Molecular Catalysis A: Chemical 262 (2007) 190–215
JOURNAL OF MOLECULAR CATALYSIS A: CHEMICAL
www.elsevier.com/locate/molcata

Polyoxometalate-based homogeneous catalysis of electrode reactions: Recent achievements

Bineta Keita, Louis Nadjo *

Laboratoire de Chimie Physique, Groupe d'Electrochimie et de Photoélectrochime, UMR 8000, CNRS, Université Paris-Sud, Bâtiment 350, 91405 Orsay Cedex, France

Available online 5 September 2006

Abstract

Polyoxometalates (POMs) constitute a broad family of molecular oxides showing promise in several efficient and clean electrocatalytic processes, when they are handled in appropriate conditions. Reduction and oxidation possibilities exist as well. The present short focused review shows the usefulness of POMs in selected electrocatalytic processes. Quantitative transformations were demonstrated in several examples, including hydrogen production, NO_x reduction, dioxygen reduction, coenzyme oxidation... This selection leaves room for a wealth of other possibilities. It appears clearly that several parameters must be taken into account in the design and study of these processes. Among them, the stability in aqueous or non aqueous solutions is an absolute prerequisite, which excludes the use of several newly synthesised fragments solely stable in the solid state. New parameters, in addition of those highlighted here, might emerge because POMs with new atomic compositions, new structures and new reactivities, continue to be synthesised and characterised. The challenge, however, is to find new POMs or new POM-based systems to decrease overpotentials which remain high for most reactions and improve the overall kinetics.

Finally, an optimistic prediction is that POMs, owing to their versatility and possibility to accommodate nearly all the atoms of the periodic classification, will become popular to drive selected electrocatalytic processes.

Keywords: Polyoxometalates; Heteropolyanion; Isopolyanion; Transition Metals; Sandwich-type Polyoxometalates; Electrocatalysis; Cooperativity

1. Introduction

Polyoxometalates (POMs for convenience) are anionic structures constituted of early transition-metal elements in their highest oxidation state, hence their usual designation as early transition-metal–oxygen-anion clusters. They are remarkable in several respects, including the multitude of their properties based on their sizes, shapes, charge densities and reversible redox potentials or their enormous diversity of structures. In the following, POM will be kept as the general term, but other designations like isopolyanions (IPAs) and heteropolyanions (HPAs) might also be used occasionally. The structures of the vast majority of POMs studied in electrochemistry are primarily derived from the Keggin structure and the Wells–Dawson structure.

POMs constitute a versatile family of molecular metal-oxide clusters with applications in catalysis as well as in medicine and material science, hence the unabated interest in their redox, catalytic and electrocatalytic properties [1–15]. In particular, their redox behaviours may be very flexible and finely tuned on purpose, by changing smoothly their composition, with a tremendously diverse variety of structures [5]. Most of their properties have been described in a series of excellent reviews, which usually include short developments on their electrochemistry and redox catalysis properties [1–9,16–20]. The reader is referred to these reviews for general descriptions of POM synthesis, structures and reactivity. Among these reviews, particular attention is drawn to those few containing substantial developments on electron transfer behaviours and the electrochemistry of POMs [1,3,4,6–9,16–20].

The present paper focuses on the homogeneous catalysis of electrode reactions by POMs. As a matter of fact, oxidised forms of POMs may only accept electrons; in contrast, their reduced forms, owing to their electron and proton transfer and/or storage abilities, may behave as donors or acceptors of several electrons while maintaining their structure. As a consequence, most POMs may be considered as close mimics of mixed metal oxides and therefore, be studied as their soluble analogues, at least as concerns their catalytic properties in photochemistry and elec-

* Corresponding author. Tel.: +33 1 69 15 77 51; fax: +33 1 69 15 43 28.
E-mail address: nadjo@lcp.u-psud.fr (L. Nadjo).

1381-1169/$ – see front matter © 2006 Elsevier B.V. All rights reserved.
doi:10.1016/j.molcata.2006.08.066

trochemistry. In addition, the impetus for the catalytic studies of transition metal cation-substituted POMs was triggered by the seminal remark of Baker [21] that monosubstituted POMs can be considered as the analogues of metalated porphyrins and used in catalytic processes with the advantage, relative to their organic counterparts, of thermal stability, robustness and inertness toward oxidising environments.

The purpose of the present communication is not to provide an exhaustive review of all papers in which some electrocatalytic behaviors of POMs intervene, but rather to highlight the main parameters that emerge from the scrutiny of the vast majority, if not all, of the electrocatalytic properties of these chemicals at electrodes. Thus, examples will be selected to illustrate mainly the following points: (i) examples which fall clearly in the two groups of catalytic processes to be defined shortly in this section; (ii) the outcomes of POM super structures as concerns improvements and/or new catalytic processes like the reduction of nitrate or nitrogen protoxide; (iii) cooperativity between metallic centers within the POM framework (Mo-Fe or Mo-Cu centers), a newly described feature, which is, however, already encountered in biological systems.

With these ideas in mind, examples described in the following are selected to highlight the main parameters cited in the foregoing section. Survey of the literature indicates that most relevant papers, not devoted to chemically modified electrodes, are covered in recent reviews. Even if new examples turn out to come mostly from the work carried out in the present authors' laboratories during the last few years, due examination of some relevant papers from other groups are included.

Possibilities of electrocatalysis of reactions at electrodes are among the powerful incentives for the electrochemical study of POMs. Interesting results were obtained both in electrocatalytic reductions and oxidations, provided the appropriate form of the POM is used. Three recent reviews devoted to the electrochemical properties of polyoxometalates, in particular as electrocatalysts, are available [7–9]. The last one focuses more specifically on electrocatalysis on modified electrodes. In the present text, attention will be drawn specially to the basic principles that could be considered to govern most of solution processes.

The term "electrocatalysis" will be used frequently to describe POM-based homogeneous catalysis of electrode reactions. Strictly speaking, electrocatalysis applies to the "dependence of the electrode reaction rate on the nature of the electrode material" [22]. In the following, this term will be used in a broader sense and will be admitted to include the possibility that the catalyst be homogeneously dissolved in the electrolyte solution as well as the case where the catalyst is attached to the electrode surface. A short chapter on the electrocatalysis of inorganic chemicals by chemically modified electrodes can also be found in Vol. 10 of the *Encyclopedia of Electrochemistry* [9]. Therefore, this domain will not be covered in the following. Particular attention is exercised toward the literature covering the period from 1996 to 2005 to provide a satisfactory overlap with the recent reviews [7,8] devoted to the electrochemistry of POMs and to their properties as electrocatalysts.

After a short illustration, by appropriately selected examples, of the two basic nuances of electrocatalytic processes, the paper will analyse the case of vanadium-substituted polyoxotungstates as versatile catalysts. The third and fourth sections will consider, respectively, the influence of the nature and number of, eventually active, sites within the POM framework and the eventual cooperativity between these centers.

2. Experimental illustration of the basic concepts of homogeneous catalysis of electrode reactions

Modeling the homogeneous catalysis of electrode reactions will be described succinctly here for a reduction process. In that case, electron exchange occurs in solution between the reduced catalyst and the substrate, thus regenerating the catalyst and explaining the observed catalytic effect. Transposition to oxidation processes is straightforward. In short, electron transfers to or from a molecule must be viewed as a succession of elementary electrochemical and chemical reaction steps. Such simplified reaction schemes served as the basis for theoretical analysis of catalytic phenomena. The analysis, which is sketched in more detail in an Appendix A, highlights two main mechanistic nuances of the catalysis: (i) the first one considers only the possibility of simple solution electron transfers. The catalyst constitutes an electron shuttle between the electrode and the solution, where it is engaged in a direct redox electron transfer with the substrate. This type of catalysis is termed *redox catalysis*; (ii) the second pathway goes through the formation of an adduct. In this case, the reduced form of the catalyst builds up with the substrate a relatively unstable adduct, which then decomposes, eventually after further reduction at the electrode surface or in solution. Finally, either the oxidized form of the catalyst or its reduced form is regenerated. This type of catalysis is termed *chemical catalysis*.

2.1. Electrocatalytic oxidation of NAD(P)H by POMs: an example of redox catalysis

Recently, much efforts were devoted to the study of oxidation of NAD(P)H by POMs [23–28].

The incentive for this research is the known importance of NAD(P)H/NAD(P)$^+$ redox couples in biological systems as well as the possibility of developing amperometric biosensors for NAD(P)$^+$-dependent dehydrogenases. As a consequence, both enzymatic synthesis [29] and electrochemical regeneration [30] are relevant. In this search, the stability of the reaction products in the presence of each other is also a necessary condition for usefulness.

The work described in the following constitutes an illustrative example in which mechanistic issues are probed in detail, including kinetics, elementary reaction pathways, bulk electrolysis performance and stability issues.

Here, focus is directed toward the oxidation of NADH. Quantitative studies in fairly acidic solutions are precluded by the known rapid hydration of NADH below pH 6. Nadjo and Keita succeeded in synthesising and/or selecting POMs stable in neutral or alkaline media and likely to meet all the necessary criteria. These authors demonstrated an efficient oxidation of NADH by several vanado-tungsto phosphoric heteropolyanions, stable at

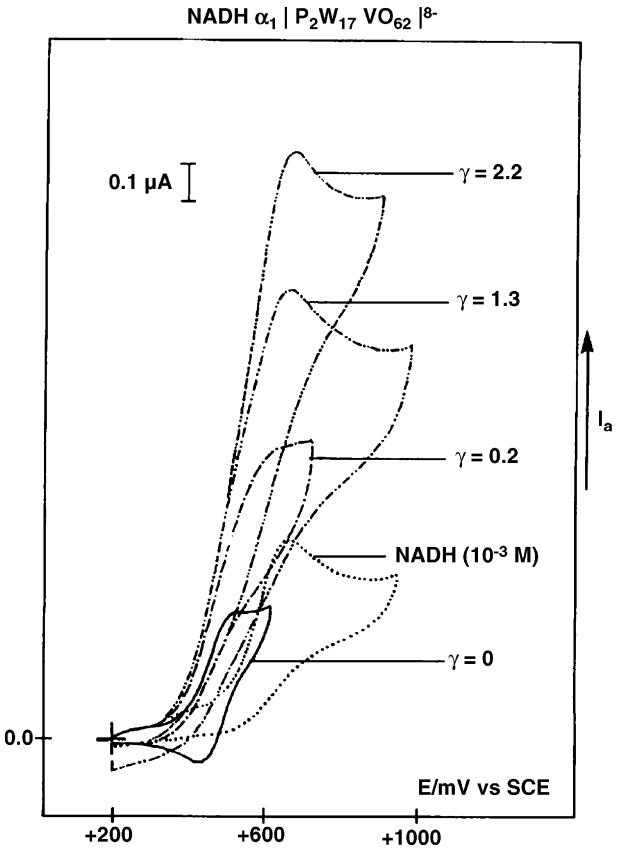

Fig. 1. Cyclic voltammograms obtained for the system $\alpha_1P_2VW_{17}O_{62}{}^{8-}$/NADH. Electrolyte pH 7 phosphate buffer. Reference electrode SCE; working electrode: 1 mm diameter Pt disk. The solutions contain 10^{-3} M $\alpha_1P_2VW_{17}O_{62}{}^{8-} + 10^{-3}$ γ M NADH, except for the one containing 10^{-3} M NADH alone. Scan rate $v = 5\,mV\,s^{-1}$ (taken from Ref. [27]).

pH 7 [23–27]. The stability of the mixtures was established. In addition, complete regeneration of NADH was obtained from NAD^+ in the mixtures with the heteropolyblue (HPB) in the presence of alcohol dehydrogenase (ADH) and ethanol. The correct stoichiometry of NADH to POM was found, by spectrophotometry and coulometry, to be 1:2, thus indicating that the POM acts as a one-electron oxidant. These observations support the following overall reaction scheme:

$$2\alpha_2 - [P_2VW_{17}O_{62}]^{7-} + NADH \leftrightarrows 2\alpha_2 - [P_2VW_{17}O_{62}]^{8-} + NAD^+ + H^+$$

More detailed mechanistic characteristics establish the purely redox catalysis behavior of the systems studied. Typically, the system NADH/α_1-$[P_2VW_{17}O_{62}]^{7-}$ is shown in Fig. 1 as a representative example of cyclic voltammetry evolution at a scan rate of $5\,mV\,s^{-1}$. The excess parameter ($\gamma = C^\circ_{NADH}/C^\circ_{POM}$) values appear on each curve from $\gamma = 0$ (first one-electron diffusion-controlled process of the POM) to $\gamma = 2.2$ (electrocatalytic process). The direct oxidation of NADH on the glassy carbon electrode surface is also shown for comparison. The evolution of the CVs is easily understood on the basis of a fast oxidation of NADH by the oxidized form of the POM. The same overall pattern is obtained for other suitable POMs. Qualitatively, the intensity of the catalytic wave is observed to depend on the formal potential of each POM. This constitutes a first indication that the process might follow a purely redox catalysis behaviour. Rate constants of the catalytic process were measured by double potential step chronocoulometry [31] under pseudo first order rate conditions. These values are gathered in Table 1. Excellent agreement was obtained for the rate constant values cross-checked by the stopped flow technique [24]. The results are gathered in Table 1 and Fig. 2. The plot of $\log_{10} k$ as a function of the one-electron redox potentials of the POMs in Fig. 2 is featured by a straight line with a slope of $16.4\,V^{-1}$. This observation allows to write and discuss a detailed mechanistic pathway (Scheme 1).

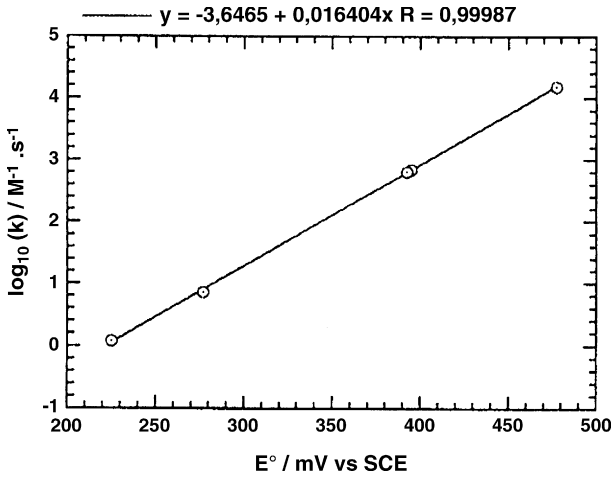

Fig. 2. Plot of log k *vs.* the one-electron redox potentials E° of the POMs (taken from Ref. [27]).

It is shown first that hydride transfer is not a likely reaction pathway. The rate limiting step is established to be the initial one-electron transfer by using rate constants obtained by independent measurements. Then to go deeper into the mechanism, the initial one-electron rate-limiting step was developed into three successive steps (Scheme 2) in which (NADH, HPA) and ($NADH^{\bullet+}$, HPB) represent the reactants in their reaction

Table 1
Standard potential for the first redox system of each POM and second order rate constant k derived from DPSC experiments on HPB/NADH systems at pH 7

HPB	α_1-$P_2W_{17}VO_{62}{}^{8-}$	α_1-$P_2W_{17}MoO_{62}{}^{7-}$	α_2-$P_2W_{17}VO_{62}{}^{8-}$	$P_2W_{16}V_2O_{62}{}^{9-}$	α_2-$P_2W_{17}MoO_{62}{}^{7-}$
E° (mV *vs.* SCE)	477.5	395.5	392.5	277.5	225
γ	10	10	10	10	20
k ($M^{-1}\,s^{-1}$)	1.5×10^4	6.9×10^2	6.4×10^2	7.1	1.2

Each value of k is the average of at least five experiments. The values of γ are not necessary, but have been added to give a better idea of the experimental conditions (taken from Ref. [27]).

$$(\text{HPB} - \text{le} \rightleftharpoons \text{HPA}) \qquad (0')$$

$$\text{NADH} + \text{HPA} \underset{k_{-1}}{\overset{k_1}{\rightleftharpoons}} \text{NADH}^{\bullet+} + \text{HPB} \qquad (1)$$

$$\text{NADH}^{\bullet+} + \text{B} \underset{k_{-2}}{\overset{k_2}{\rightleftharpoons}} \text{NAD}^{\bullet} + \text{BH}^{+} \qquad (2)$$

$$\text{NAD}^{\bullet} + \text{HPA} \underset{k_{-3}}{\overset{k_3}{\rightleftharpoons}} \text{NAD}^{+} + \text{HPB} \qquad (3)$$

Scheme 1.

sites, whereas NADH + HPA and $NADH^{\bullet+}$ + HPB represent the reactants and products beyond the average distance of diffusion; k_{diff} is the diffusion-limited rate constant, k_{1act} and k_{-1act} are the activation-controlled rate constants. Each of these steps could be, in principle, rate-limiting [32]. However, the experimental results in Fig. 2 indicate that the diffusional separation of the HPB/$NADH^{\bullet+}$ pair is rate limiting without any tendency to observe a rate-limiting electron hop. A value of $E^{\circ} = +0.80$ V was determined for the NADH/$NADH^{\bullet+}$ couple at pH 7. These results establish that a purely redox catalytic process is operative. A short study, in more alkaline media, devoted to the electrocatalytic oxidation, by selected POMs, of NADPH [28], a substrate closely related to NADH, with the same importance in vivo and in vitro, was also successful and shows the same trends. A rate constant $k = 3.5 \times 10^3\ M^{-1}\ s^{-1}$ was measured for the system $P_2V_2W_{16}$/NADPH at pH 8. However, study of such systems is not yet pursued with the same wealth of rate constant measurements as for NADH.

2.2. An example of chemical catalysis: the reduction of nitrite

The electro-assisted chemical catalysis of the reduction of nitrite and nitric oxide constitutes an example in which the mechanistic issues are unravelled in detail for a Fe^{III}-substituted POM [33]. As concerns excellent bulk electrolysis performance and POM stability issues, the only example, to our knowledge, is the demonstration, carried out by our group, of quantitative conversion of NO into N_2O by $[P_2Mo_{18}O_{62}]^{6-}$ and other selected POMs in aqueous media [10]. These issues are analyzed in this section.

The detailed mechanistic pathway given by Toth and Anson [33] for the electrocatalytic reduction of nitrite by Fe^{III}-substituted Keggin-type POMs establishes unequivocally the chemical catalysis scheme operative in this system. Specifically, the proposed catalysts can be represented by the general formula:

$$\text{NADH} + \text{HPA} \underset{k_{diff}}{\overset{k_{diff}}{\rightleftharpoons}} (\text{NADH, HPA})$$

$$\underset{k_{-1}\,act}{\overset{k_{1}\,act}{\rightleftharpoons}} (\text{NADH}^{\bullet+}, \text{HPB})$$

$$\underset{k_{diff}}{\overset{k_{diff}}{\rightleftharpoons}} \text{NADH}^{\bullet+} + \text{HPB} \qquad (4)$$

Scheme 2.

α-$XW_{11}O_{39}Fe^{III}(H_2O)^{n-}$ (X = Si, Ge, $n = 5$; X = P, As, $n = 4$). A Fe-nitrosyl complex, formed upon reduction of the Fe center, was detected and characterized. The actual catalytic process to obtain ammonia occurs at more negative potentials where the necessary number of charges is accumulated and delivered by the W-framework. The overall mechanism up to the Fe-nitrosyl formation involves the following steps [33]:

$$2\alpha\text{-}XW_{11}O_{39}Fe^{III}(H_2O)^{n-} + 2e^{-} \leftrightarrows 2\alpha\text{-}XW_{11}O_{39}Fe^{II}(H_2O)^{(n+1)-}$$

$$2\alpha\text{-}XW_{11}O_{39}Fe^{II}(H_2O)^{(n+1)-} + NO_2{}^{-} + 2H^{+} \leftrightarrows 2\alpha\text{-}XW_{11}O_{39}Fe^{II}(NO)^{(n+1)-} + 2\alpha\text{-}XW_{11}O_{39}Fe^{III}(H_2O)^{n-} + H_2O,$$

$$X = Si, Ge, n = 5; X = P, As, n = 4$$

The following two processes: $HNO_2 \leftrightarrows H^{+} + NO_2{}^{-}$ $pK_a = 3.3$ at 18 °C and slow disproportionation of HNO_2 in fairly acidic solution: $3\ HNO_2 \leftrightarrows HNO_3 + 2NO + H_2O$, indicate that nitrous acid might be the reactive intermediate, depending on the pH domain explored. Finally, a loss in selectivity and a low yield [33] are attributed to electrode surface derivatization [20].

Actually, as concerns the electrocatalytic reduction of nitrite and nitric oxide, redox catalysis and chemical catalysis pathways cannot always be delineated sharply. As a matter of fact, Keita et al. [34,35] demonstrated, at the same time that Toth and Anson were establishing the aforementioned mechanism [33], that this catalytic process is observed with a large variety of POMs, including several plenary unsubstituted ones and even lacunary species. For example, a supramolecular compound like $[P_8W_{48}O_{184}]^{40-}$, with only W centers, can also be used to reduce NO efficiently without derivatization of the electrode surface [36].

Fig. 3 and Table 2 illustrate the main results of interest in the present context. In Fig. 3, only the phenomena associated with the first redox wave of $[P_2Mo_{18}O_{62}]^{6-}$ selected as a representative example, are shown. In the absence of this POM, nitric oxide is reduced close to the supporting electrolyte discharge. The substantial improvement brought about by the presence of $[P_2Mo_{18}O_{62}]^{6-}$ is immediately obvious on Fig. 3. Several other POMs show the same kind of catalytic effects on their respective first redox couples in the presence of NO. A list of those tested in this issue can be found in the original paper [10] and in the patents [34,35]. A quantitative evaluation of the improvement is presented in Table 2 through the parameter ΔE_i, defined as the difference between the potentials values at which an arbitrarily fixed current density of 53 $\mu A\ cm^{-2}$ was observed in the presence and absence of POM, provided the catalyst current was substracted [10]. Indeed, very large ΔE_i values are achieved in these experiments. In Table 2 are also gathered the results of preparative scale electrolyses from which sizeable amounts of chemicals can be detected and quantified. N_2O was the only product detected. It turned out that the yields for N_2O production were close to 100% for all the POMs studied. In short, these yields seem to be independent of the reduction potentials of the

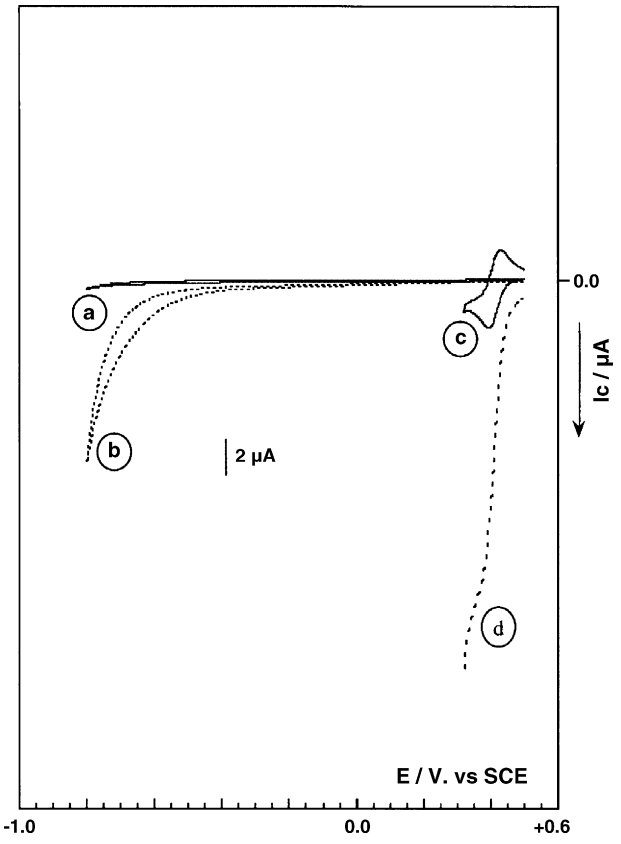

Fig. 3. Cyclic voltammograms run in a pH 1 medium (0.2 M $Na_2SO_4 + H_2SO_4$) at a scan rate of 10 mV s^{-1}. Working electrode: 5 mm diameter glassy carbon disk; solutions deoxygenated with pure argon: (a) supporting electrolyte alone; (b) supporting electrolyte saturated with NO; (c) supporting electrolyte wit 10^{-4} M $[P_2Mo_{18}O_{62}]^{6-}$ thoroughly deaerated with argon; (d) solution (c) saturated with NO (taken from Ref. [10]).

POMs used in this work. This feature suggests strongly a chemical catalysis pathway for the electrocatalytic reduction of NO by the present POMs. The detailed succession of electrochemical and chemical sequences occurring during the reaction remains a challenging problem.

Table 2
Reduction of NO into N_2O by selected one- and two-electron reduced POMs

POM (number)	Electrolysis potential *vs.* SCE/V	ΔE_i/V[a]	Yield (%)[b]
$\alpha_1[P_2W_{17}MoO_{62}]^{6-}$ (1)	+0.1	1.080	103 ± 6
$[P_2W_{18}O_{62}]^{6-}$ (2)	−0.06	0.810	100 ± 6
$[P_2Mo_{18}O_{62}]^{6-}$ (3)	+0.32	1.200	100 ± 6
$[SiMo_{12}O_{40}]^{4-}$ (4)	+0.18	1.070	98 ± 6
$[P_2W_{12}Mo_6O_{62}]^{6-}$ (5)	+0.05	1200	95 ± 6

Adapted from reference [10]. The reduction of each POM is carried out on its first redox wave. The POMs numbered 1 and 2 are reduced by one electron per molecule, and the other ones by two electrons.

[a] Improvement in the operational potential ΔE_i obtained for the reduction of NO in the presence of the various POMs in pH 1 medium (0.2 M $Na_2SO_4 + H_2SO_4$). The values are measured for a current density of 53 µA cm^{-2} after substraction of the POM current. This current density, in the absence of POM, is obtained at −0.8 V *vs.* SCE for NO saturated solutions. Glassy carbon working electrode surface area: 0.19 cm^2; $\gamma = [NO]/[POM] = 15$.

[b] Yield for production of N_2O per mole of HPB in the electrolysis.

Electrocatalytic behaviours are frequently explored, especially for new POMs,. Following the works of Toth and Anson [33] on the one hand, Keita et al. [34,35] on the other hand, the reduction of nitrite has become a popular electrochemical test reaction to assess the catalytic properties of new POMs, [37–40]. Many other successful electrocatalytic processes were studied and published. Most of the corresponding papers are summarised in recent reviews [7,8,41]. They include the hydrogen evolution reaction (her), the reduction of O_2, H_2O_2, DMSO, $[ClO_3]^-$, or $[BrO_3]^-$, etc.; the oxidation of DMSO, alcohols and olefins, etc.

The foregoing discussion underscores the complexity of problems. As a consequence, POM properties are studied mostly without any particular attention to actual mechanistic pathways. One possibility among the reasons that guide toward this general screening of properties before any in-depth mechanistic study, must be traced to the tremendous diversity of atomic composition, shape, structure and reactivity of POMs on the one hand and the wealth of the substrates that can be catalysed on the other hand. Therefore, even though mechanistic evidences will be stressed more often than not, the present state of the art in the homogeneous catalysis of electrode reactions by POMs will be described in the following by highlighting the main parameters and behaviours that emerge from most, if not all, recent work.

3. Vanadium-substituted Wells–Dawson-type polyoxotungstates as versatile electrocatalysts

The electrochemical pattern of most POMs useful for electrocatalysis studies is generally featured by the chemical reversibility of the first or the first several redox waves, in the absence of a substrate to be catalysed. This behaviour guarantees the better stability scheme for the electrocatalyst, even though, in exceptional cases, a kinetic stability of otherwise chemically irreversible processes, might be envisioned. As a consequence, oxidised forms of POMs may accept electrons and behave as oxidation catalysts; in contrast, their reduced forms, owing to their electron and proton transfer and/or storage abilities, may behave as donors or acceptors of several electrons, thus acting mainly as reduction catalysts. This versatility of electrocatalytic behaviors of POMs is usually obtained through electrochemical manipulation of their redox centers. However, in favourable cases, this dual capability might be built-in during the synthesis of POMs containing mixed valence centers. This paragraph presents different nuances of this dual behaviour illustrated by vanadium-substituted Wells–Dawson-type polyoxotungstates.

The substitution of vanadium, eventually accompanied by molybdenum, into a W framework of a POM is the focus of this study [28]. The substitution of vanadium into the framework of a tungstic or molybdo-tungstic POM increases the negative charge of the anion and is, therefore, expected to shift the stability of the saturated species to higher pH. Several prominent properties are also recognized for vanadium compounds in general, including polyoxovanadates and vanadium-substituted POMs. Synthesis, characterization, electronic structures and catalytic behaviours of vanadium-substituted POMs have generated a vast literature [42–59]. Specifically, electrocatalytic processes were illustrated both in reductive and in oxidative reactions. The electroreduc-

tion of nitric oxide and nitrite in a pH 2 medium was efficiently carried out by reduced α_1-$[P_2VW_{17}O_{62}]^{7-}$ [39]. Regarding oxidation reactions, the efficient catalysis of the oxidation of NAD(P)H by several vanado-tungsto-phosphoric POMs was described in a previous section [23–28].

New results allow to develop and expand several aspects of the electrochemistry and electrocatalytic behaviours of vanadium-substituted POMs [28]. Their dual possibilities will be illustrated by the oxidation and reduction of nitrogen oxides, merely by modifying the redox state of the vanadium center within the same POM. In a selected series of P- and As-Wells–Dawson type derivatives, emphasis is put on the stability domain and complete characterization of $[P_2V_2W_{16}O_{62}]^{8-}$ ($P_2V_2W_{16}$ for short) as a representative example, because the redox potential of the vanadium center within this POM is particularly suited for several electrocatalytic processes.

3.1. Stability of selected V-substituted POMs

Table 3 indicates the stability domains for all the derivatives. These domains were obtained by monitoring their UV–vis spectra between 600 and 200 nm as a function of pH over a period of at least 24 h. Fine small dots indicate the domain in which a particular derivative is stable; vertically hatched domains correspond to a decomposition less than or equal to 20%; finally, clear domains indicate a decomposition of between 20 and 40%. Several molecules in their oxidized form remain stable up to pH 7 and further. As expected, the presence of the V-center enlarges the pH stability domain of these mixed addenda heteropolytungstates in comparison with the corresponding monometal main precursors $[X_2W_{18}O_{62}]^{6-}$ (X = P or As) and the corresponding Mo-substituted derivatives. Using the same reasoning, it is also expected that the reduced forms of these molecules should be stable up to the same or even higher pH values than the corresponding oxidised forms. A complementary cross-check of this suggested stability was obtained by cyclic voltammetry experiments which usually cover a duration as long as 8–10 h. Perfect reproducibility of the time-to-time run of the voltammogram for a selected potential scan rate was taken as a complementary stability criterion.

Table 3
Stability monitored by UV–visible spectroscopy over 24 h, for selected V-substituted Wells–Dawson POMs. The numbering of metallic atoms follow the IUPAC recommendations

HPA[b] *(abbreviation)*	pH			
	0 - 5	6	7	8
α_1-$[As_2VW_{17}O_{62}]^{7-}$ (α_1–$As_2V^{(+V)}W_{17}$)	■	▨		
α_1-$[P_2VW_{17}O_{62}]^{7-}$ **(α_1–$P_2V^{(+V)}W_{17}$)**	■	■	■	
α_2-$[As_2VW_{17}O_{62}]^{7-}$ **(α_2–$As_2V^{(+V)}W_{17}$)**	■	■	■	
α_2-$[P_2VW_{17}O_{62}]^{7-}$ **(α_2–$P_2V^{(+V)}W_{17}$)**	■	■	■	
1, 2, 3-$[As_2Mo_2VW_{15}O_{62}]^{7-}$ **$As_2Mo_2V^{(+V)}W_{15}$**	■	▨		
1, 2, 3-$[P_2MoV_2W_{15}O_{62}]^{8-}$ **($P_2MoV_2^{(+V)}W_{15}$)**	■	■	▨	
1, 2, 3-$[P_2V_3W_{15}O_{62}]^{9-}$ **($P_2V_3^{(+V)}W_{15}$)**	■	■	■	
1, 2-$[P_2V_2W_{16}O_{62}]^{8-}$ **($P_2V_2^{(+V)}W_{16}$)**	■	■	■	

Adapted from reference [28]. (■) Stable; (▨) <20% transformation; (□) 20–40% transformation. [a]References corresponding to synthesis and characterisation of these POMs can be found in the original paper [28]; for further details, see text.

3.2. Electrochemistry of $P_2V_2W_{16}$ and the other V-substituted POMs

The voltammetric behaviour of $P_2V_2W_{16}$ is selected as a representative example to illustrate the wealth and variety of the electrochemistry of V-centers within these POMs. Fig. 4A shows the cyclic voltammogram (CV) of this complex in a pH 5 acetate medium. The two most positive waves in Fig. 4A feature one-electron processes and are attributed to vanadium centers [60]. Their potential locations are substantially positive to that of processes attributed to W centers. In the following, attention is focused on the electrochemical behaviors of V-centers. Fig. 4B and C complete Fig. 4A to give a detailed picture of the evolution of the V-waves as a function of pH. Starting from the pH 5 medium, the two waves move in the positive potential direction as the pH is decreased and, finally, visually merge. However, a clear evolution in peak current intensities and peak widths is still observed between pH 1 and 0. A striking evolution of the voltammetric pattern was observed between pH 5 and 8 as appears from comparison of Fig. 4A and C. The second V-wave is shifted in the negative potential direction and becomes drawn-out and largely irreversible. It is worth noting that the potential location of the first V-wave can be considered to remain fixed in this pH domain. Actually, this independence from pH was observed roughly from pH 4 to higher values. In short, the observed voltammetric pattern can be explained in the following manner: for pH < 4, the first V-wave shows classical potential shifts as a function of acidity and, then, becomes pH-independent for higher pH values; in contrast, the second V-wave experiences much larger displacements, whatever the pH from 0 to 8, a behaviour that induces the coalescene or separation of the two V-waves.

Table 4 gathers the reduction peak potentials and the apparent formal potentials measured at pH 7 for the V-substituted Wells–Dawson POMs studied in this work. Combination of this diversity in the number of V atoms with the presence of As or P as the central heteroatom in these tungstic and molybdotungstic structures modulates substantially the apparent formal potentials measured at pH 7 for the first V-wave. The formal redox potentials taken as an average of the cathodic and anodic peak potentials span the range from +569 mV to +122 mV. This leaves considerable flexibility in the choice of POMs for electrocatalytic purposes. However, it might be misleading to consider only formal potentials, which must be completed by the comparisons of the actual behaviors of the voltammetric patterns. The morphologies of the cyclic voltammograms should indicate, at least qualitatively, the differences in overall acid–base properties within complexes and their influence on the CVs. As an example, it was demonstrated that the beneficial influence expected

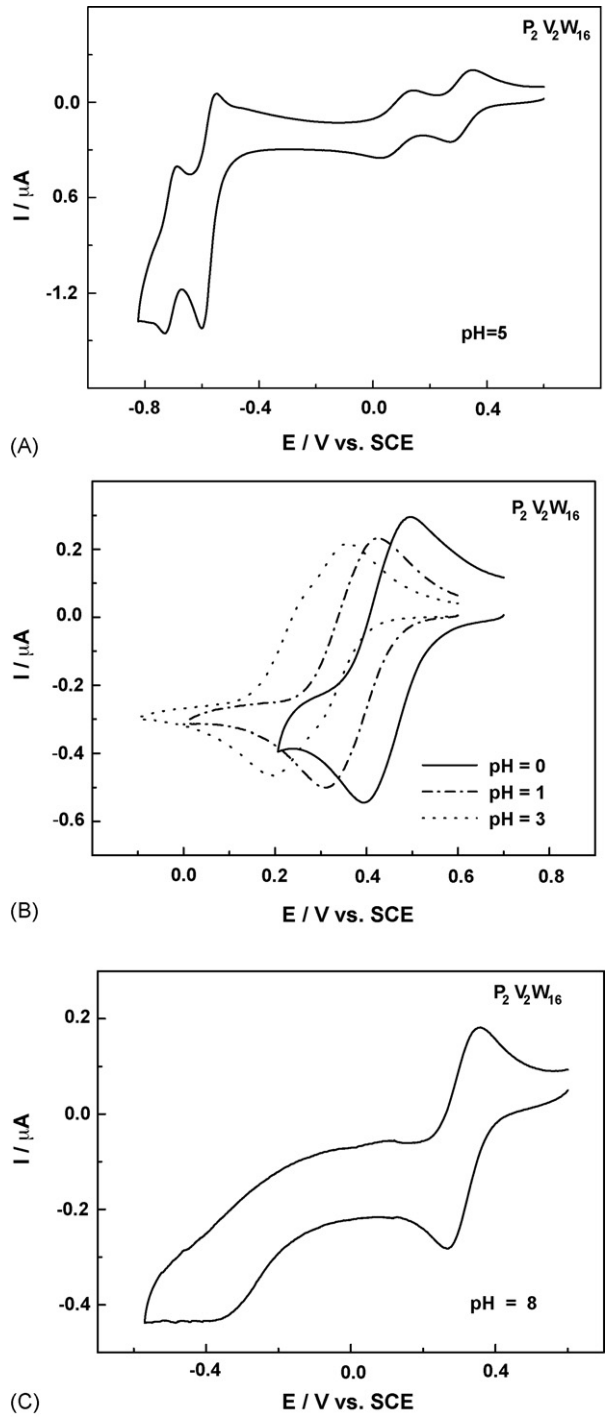

Fig. 4. Cyclic voltammograms (CVs) of 2×10^{-4} M $P_2V_2W_{16}$ in various media. The scan rate was 2 mV s^{-1}, the working electrode was glassy carbon, and the reference electrode was SCE. (A) Pattern showing the two V-Waves and two W-waves at pH 5 (1 M $CH_3COONa + CH_3COOH$). (B) Evolution of the two V-waves as a function of pH. Compositions of the media: pH 0: H_2SO_4; pH 1 to 3:0.5 M $Na_2SO_4 + H_2SO_4$. (C) CV showing the two V-waves at pH 8:50 mM TRIS + 0.5 M $Na_2SO_4 + H_2SO_4$ (taken from Ref. [28]).

from accumulation of V-centers in $P_2V_3W_{15}$ as compared to $P_2V_2W_{16}$ and $P_2MoV_2W_{15}$ might be counterbalanced by the qualitatively poorer acid–base and electron transfer abilities of the former complex [28].

Table 4
V-reduction peak potential E_{pc1} and apparent formal potentials $E^{\circ\prime}$ (defined as $(E_{pc1} + E_{pa1})/2$) measured in a pH 7 medium by cyclic voltammetry for a selection of V-substituted Wells–Dawson POMs

Complex	E_{pc1} (mV)	$E^{\circ\prime}$ (mV)
α_1-As_2VW_{17}	531	569
α_1-P_2VW_{17}	453	504
α_2-As_2VW_{17}	404	446
α_2-P_2VW_{17}	377	414
$As_2Mo_2VW_{15}$	455	489
$P_2V_3W_{15}$	59	122
$P_2V_2W_{16}$	255	298
$P_2MoV_2W_{15}$	267	309

Taken from Ref. [28]. Scan rate of 2 mV s^{-1}; reference electrode: SCE; working electrode: glassy carbon.

3.3. Electrocatalytic processes based on V-substituted POMs

3.3.1. Electrocatalysis of the reduction of nitrite: recent improvements

Electrocatalytic reduction of nitrite by reduced POMs has been studied for some time and described in a previous section. Examples concerning specifically V-substituted POMs were also studied [39,61]. General aspects of such electrocatalytic processes were discussed recently [62]. The example presented here is aimed at illustrating the continuous improvement brought about in this reaction by the use of appropriately selected POMs [28]. Fig. 5 shows the current enhancement accompanying the addition of $NaNO_2$ to a pH 1 solution of $P_2V_2W_{16}$ (*vide supra* for the behaviour of $NaNO_2$ in this medium).

The pH 1 value was selected because it ensures a fairly complete merging of the two V-waves of this complex. The current intensity increase is observed readily at the reduction potential of the V-centers for a modest increase of γ values (γ is the excess parameter defined as $\gamma = C^{\circ}_{NO_x}/C^{\circ}_{POM}$). In this potential domain, no direct reduction is observed for NO or HNO_2 present in the solution [10,39]. It is worth noticing the high effi-

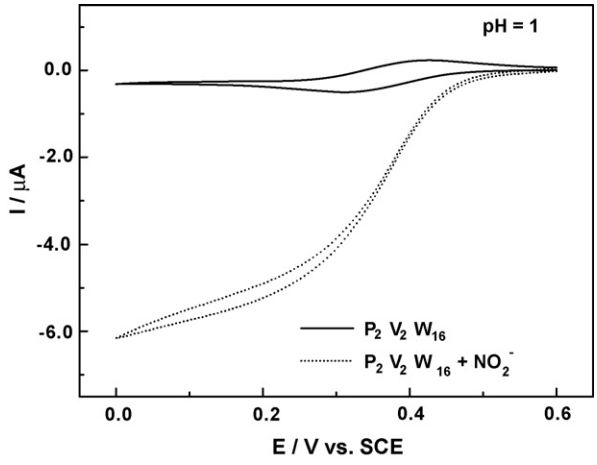

Fig. 5. Cyclic voltammetry study of the electrocatalytic reduction of 2×10^{-2} M $NaNO_2$ ($\gamma = 100$) with a 2×10^{-4} M solution of $P_2V_2W_{16}$ in a pH 1 medium (0.5 M $Na_2SO_4 + H_2SO_4$). The scan rate was 2 mV s^{-1}, the working electrode was glassy carbon, and the reference electrode was SCE (taken from Ref. [28]).

ciency of the electrocatalysis and the fairly positive potential at which it takes place. The main incentive to show Fig. 5 is to stress the possibility that an appropriate selection of POMs could be performed to obtain a continuous shift in the positive direction of the potential at which such electrocatalysis is observed. The limit is the possibility that nitrite be oxidized into nitrate by the POM instead of undergoing an electrocatalytic reduction process. This point is considered in the following. Before closing this sub-section, a short remark is in order: both vanadium- and molybdenum-substituted species show electrocatalytic beaviours at exceptionally positive potentials. The results of vanadium-substituted POMs must be associated with their better long term stability under electrocatalysis conditions.

3.3.2. Oxidative electrocatalytic processes

3.3.2.1. An example of mediated oxidation process: oxidation of nitrite. Formal potentials in Table 4 guided toward the selection of POMs likely to oxidise nitrite in a pH 7 medium [28]. Upon mixing of one of the selected POMs with nitrite at pH 7, colour changes were eventually observed as a function of time, thus indicating that the POM was acting as an oxidant. A representative experimental example is illustrated by the addition of a fixed excess of nitrite (defined by γ, *vide supra*) to a pH 7 solution of α_1-P_2VW_{17}. The evolution of the mixture was monitored by UV–vis spectroscopy between 1300 and 400 nm. Fig. 6 shows a set of spectra. Starting with the neat POM ($\gamma = 0$), addition of nitrite ($\gamma = 100$) results in the reduction of the V-center and the gradual development of the known spectrum of the reduced POM. This spectrum is the same as that of the heteropolyblue prepared by electrochemical reduction. Interestingly, it is fairly different from that of the oxidized form. A sharp isosbestic point indicates a neat conversion of one form into the other. The set of spectra in Fig. 6 was exploited to calculate a pseudo-first order rate constant $k' = 1.1 \times 10^{-3}\ s^{-1}$ under the assumption that the rate is first order in POM concentration. Table 5 gathers the main qualitative observations with the selected POMs. Despite their mostly qualitative character, the results suggest two main parameters to be operative in this issue, in addition of the necessary stability of the two relevant redox states of the POM: the formal potential of the POMs and the pH of the solution.

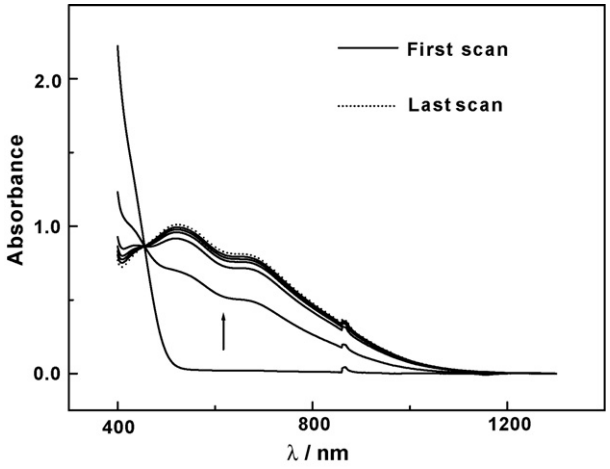

Fig. 6. Evolution of the UV–vis spectrum of a mixture of α_1-P_2VW_{17} (10^{-3} M) and $NaNO_2$ ($\gamma = 100$) in a pH 7 medium (0.4 M NaH_2PO_4 + NaOH). Starting from $t = 0$, $\gamma = 0$, time intervals between two successive spectra in the direction indicated by the arrow are, respectively: Δt (min): 2; 21; 17; 16; 28; 81 (taken from Ref. [28]).

Specifically, α_1-As_2VW_{17} is chosen as a representative example. The influence of pH might be twofold: possibly shifting the formal potential(s) of the V-wave(s) in the cases of several complexes like $P_2V_2W_{16}$; and also fixing the equilibrium state of nitrite in solution (*vide supra* for the behaviour of $NaNO_2$ in this medium), and hence the nature of the species to be actually oxidized by the POM. Then, it is conceivable that the oxidation of HNO_2 (and eventually NO) be difficult at pH 1. The first waves of α_2-As_2VW_{17} and α_1-P_2VW_{17} are located at less positive potentials than the corresponding wave of α_1-As_2VW_{17} at pH 2. Hence, the slower nitrite oxidation kinetics observed for the two former complexes. Finally, still less positive potentials measured for $P_2MoV_2W_{15}$ and $P_2V_2W_{16}$, respectively, justify that nearly no oxidation of nitrite by these POMs be obtained at pH 7. All these considerations lead to the conclusion that a redox type reaction is operative in the oxidation of nitrite by the POMs gathered in Table 5. Even though electrochemical regeneration of the catalytically active forms can be easily envisioned in favourable cases to complete an electrocatalytic cycle, the

Table 5
Qualitative evaluation of several POMs (10^{-3} M) for oxidation of nitrite ($\gamma = 200$) as a function of pH

Complex	pH	Qualitative kinetics	Isosbestic point on the spectra	Comments
α_1-$As_2V^VW_{17}$	1	Slow	Yes	Incomplete after 7 h
	2	Fast	Yes	Complete in a few minutes
	5	Fast	Yes	Complete in a few minutes
	7	Very fast	Yes	Complete in a few minutes
α_2-$As_2V^VW_{17}$	7	Slow	No	Incomplete after 7 h
α_1-$P_2V^VW_{17}$	2	Slow	Yes	Incomplete after 7 h
	5	Fast	Yes	Complete in a few minutes
	7	Very fast	Yes	The excess parameter γ must be decreased for a good observation of the isosbestic point
$P_2MoV_2W_{15}$	7	Very small conversion ratio		
$P_2V_2W_{16}$	7	Negligible conversion ratio		

Taken from Ref. [28].

present examples, due to their relative slowness, are clearly better handled by UV–vis spectroscopy for their characterization.

3.3.2.2. Reactions of V-substituted POMs with L*-cysteine.* The remarkable behaviours of several V-substituted Wells–Dawson-type POMs (stability in a large pH domain, including the physiological pH domain; stability of their oxidised (V^V) and reduced forms (V^{IV}) in the open air, formal potential of the V-center spanning a large domain, etc.) designate them as good candidates for reactions with biological systems [63]. Classical complexes of the Wells–Dawson series (α_1- and α_2-$[X_2VW_{17}O_{62}]^{7-\text{ or }8-}$ (X = As or P)) and two new dissymmetrical POMs, of general formula α_2-$[H_4XVW_{17}O_{62}]^{8-\text{ or }9-}$ (X = P or As) [64,65], with relatively low formal potentials, proved sufficiently powerful oxidants to oxidize L-cysteine. Cysteine is recognized as one of the most important among marker thiols in biological systems [66–69]. It is used in medicine and food industries. As a consequence, its detection and accurate determination constitute a valuable task and the search for sensitive and selective methods in these purposes continues unabated [66–69]. Unfortunately, classical bare solid electrodes, including bare glassy carbon electrodes, show a very slow kinetics for this process [69,70].

To guide in the choice, Fig. 7 shows the cyclic voltammograms, restricted to the V^V/V^{IV} redox couple within α_1-$P_2V^{IV}W_{17}$, α_2-$P_2V^{IV}W_{17}$ and α_2-H_4P $V^{IV}W_{17}$ in a pH 7 medium. As expected, the V^V/V^{IV} couple within α1-P_2VW_{17} is observed to have a more positive formal potential ($E^\circ = 0.506$ V) than in the α_2-P_2VW_{17} isomer ($E^\circ = 0.415$ V); finally, the V^V/V^{IV} couple within the new POM α_2-H_4PVW_{17} ($E^\circ = 0.291$ V) is the less positive of the three POMs. Among the roles assigned to catalysts, two are essential: in addition of the activation which is the primary incentive for catalysis, it is also desirable that the catalysts be selective. The problem is acute in biological systems. Specifically, for quantitative detection of cysteine in biological media, it is necessary to observe its oxidation at a potential as low as possible to avoid, eventually, interferences from currents due to the oxidation of other molecules present in complex media. Finally, the V^V/V^{IV} couples within available POMs span a formal potential domain from 0.122 V to 0.575 V [28,71]. The choice was restricted to α_2-$H_4XV^{IV}W_{17}$ (X = P or As) and α_2-$P_2V^{IV}W_{17}$ because they have the most negative formal potentials among those POMs active for the desired reaction.

Preliminary experiments performed by UV–visible–NIR spectrophotometry, allowed to obtain a linear calibration curve that suggests a clean and relatively fast transformation of α_2-$P_2V^VW_{17}$ into α_2-$P_2V^{IV}W_{17}$ through a one-electron process in the presence of increasing amounts of L-cysteine. Quantitative kinetic experiments were then performed by the stopped fow technique. The results relative to α_2-$H_4XV^{IV}W_{17}$ are selected as an illustrative example because this catalyst was analysed both by stopped flow and electrochemistry. Fig. 8 shows a representative set of spectra, after treatment for this POM. The striking observation, is a sharp isosbestic point. At the corresponding specific wavelength, its oxidized and its one-electron reduced forms appear as the only two strongly absorbing species in the mixture. Analysis of these experimental data allows to determine a rate constant $k = 925\ M^{-1}\ s^{-1}$ for the system $H_4PV^VW_{17}$-L-cysteine.

Electrocatalysis of the oxidation of cysteine was carried out in the presence of α_2-$H_4PV^{IV}W_{17}$. The formal potential of α_2-H_4PVW_{17} becomes pH-independent as soon as pH > 2.5. For a given pH, only a few millivolts variation of this E° is observed depending on the electrolyte composition. Fig. 9A shows the electrocatalysis of the oxidation of L-cysteine by α_2-H_4PVW_{17} at a glassy carbon electrode in a pH 7 medium. The following characteristics of the voltammetric pattern obtained in the presence of L-cysteine indicate unambiguously that an efficient

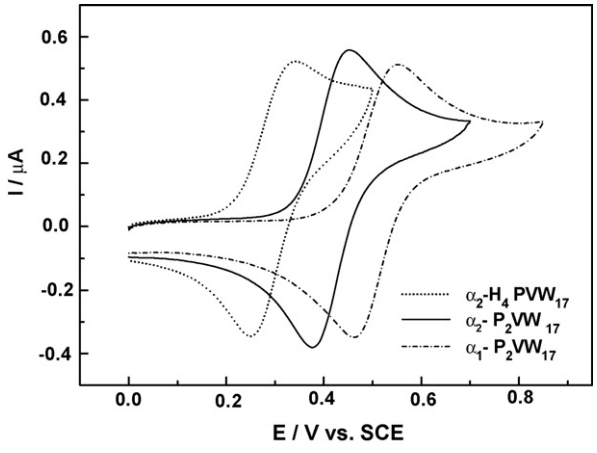

Fig. 7. Cyclic voltammograms (CVs) restricted to the V^V/V^{IV} redox couple for 2×10^{-4} M α_1-P_2VW_{17}, α_2-P_2VW_{17} and α_2-H_4PVW_{17}, respectively, run in a pH 7.00 (0.4 M NaH_2PO_4 + -NaOH) buffer solution. The scan rate was 10 mV s^{-1}, the working electrode was glassy carbon and the reference electrode was SCE. For more detailed information, see the text (taken from Ref. [63]).

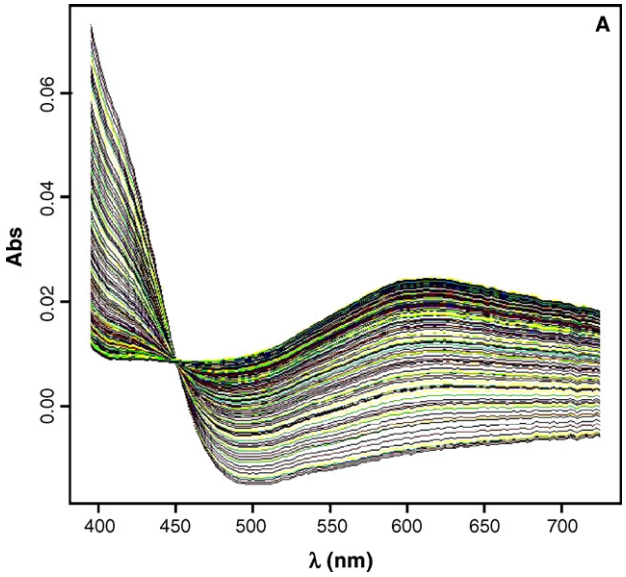

Fig. 8. Sets of UV–visible spectra of POM-L-cysteine systems as a function of time for α_2-H_4PVW_{17}. Concentrations for initial stock solutions were 0.1 mM for the POM and 1 mM for L-cysteine. The experiments were run in a pH 7.00 (0.4 M NaH_2PO_4 + NaOH) buffer solution at room temperature (taken from Ref. [63]).

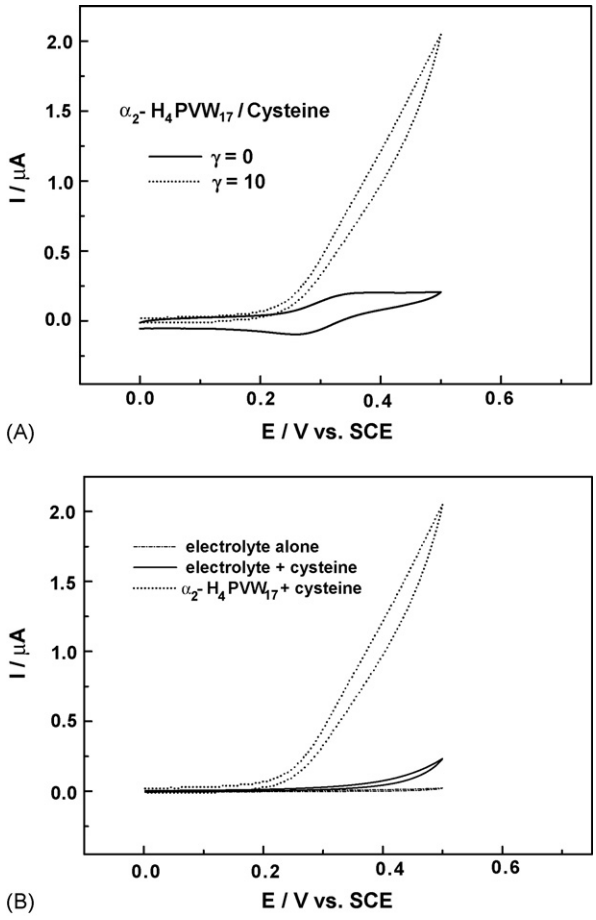

Fig. 9. Cyclic voltammetry study for the electrocatalytic oxidation of L-cysteine by 2×10^{-4} M $H_4PV^{IV}W17$, in pH 7 buffer (50 mM NaH_2PO_4 + NaOH + 1 M NaCl); the scan rate was 2 mV s^{-1}, the working electrode was glassy carbon, the reference electrode was SCE. The excess parameter was defined as $\gamma = C^{\circ}_{\text{L-cysteine}}/C^{\circ}_{\text{POM}}$. The cyclic voltammogram is restricted to the potential domain of the V^V/V^{IV} redox couple of the POM. (a) The excess parameter values were $\gamma = 0$ and $\gamma = 10$; (b) Comparison of the catalytic process ($\gamma = 10$) by $H_4PV^{IV}W_{17}$ with the background current of the supporting electrolyte and with the direct oxidation of L-cysteine on the glassy carbon electrode (taken from Ref. [63]).

electrocatalytic process is taking place with the POM: (i) a large current increase in the vanadium center oxidation domain; (ii) no reduction current observed for V^V on potential reversal. This interpretation is supported by the features displayed in Fig. 9B, where it is observed that, in the potential domain in which the catalytic current develops, the current associated with direct oxidation of L-cysteine on naked glassy carbon is small, in agreement with literature descriptions of the behaviours of this electrode material towards this thiol. For the present example, a rate constant was determined by chronocoulometry [26]. The obtained value $k = 1000\ M^{-1}\ s^{-1}$ compares very favourably with that ($k = 925\ M^{-1}\ s^{-1}$) extracted from stopped flow experiments on the same system.

A short comparison with NAD(P)H-POM systems is interesting for highlighting similarities and differences with L-cysteine-POM systems. For carefully selected POMs, both systems display a redox behavior, with good catalytic efficiency [28]. It is remarkable that selected POMs be efficient both for overall two-electron substrates (NAD(P)H) and a one-electron substrate (L-cysteine). It should also be emphasized that the follow-up reaction is different for the two systems, a deprotonation or a dimerization, respectively.

Finally, the foregoing results illustrate the two main pathways of homogeneous catalysis processes of electrode reactions. They also illustrate the possibility to manipulate the overall atomic composition and/or location of the substituent V-atom(s) in the POM framework, with the consequence that the apparent formal potentials of these centers can be made to span an appreciable potential range. A complementary behaviour is the stability of both forms of these POMs over a large pH domain, a feature that opens the way for their use in a large variety of reductive and oxidative catalytic processes. In this context, it is worth pointing out that such POMs were also used for the direct synthesis of metal nanoparticles, because they present several interesting features not available usually with other chemical reductants. For instance, the preparation of Pd° nanoparticles from $[PdCl_4]^{2-}$ was achieved [71].

4. Influence of the nature and number of substituent sites within the POM framework

Numerous examples show that the presence of substituent transition metal centers within the POM framework is not a prerequisite for the observation of catalytic or electrocatalytic activities [10,33–39,72,73]. This section will emphasise one more example of such behaviour through a brief account of the electrocatalytic activity of $K_{28}Li_5H_7P_8W_{48}O_{184}{\cdot}92H_2O$ (P_8W_{48}) for the reduction the NO_x [36]. Nethertheless, transition metal cation-substituted POMs offer sites onto which substrate to be catalysed are likely to be complexed, thus guiding toward clear mechanistic pathways.

4.1. Electrocatalytic behaviours of P_8W_{48} towards NO_x

The cyclic voltammetry patterns observed for P_8W_{48} are extremely dependent on the nature and concentration of supporting electrolytes [36]. The main behaviours are described in Fig. 10A and B. The sensitivity was taken into account as follows. Except for the pH 0.3 medium made up solely with sulphuric acid, 1 M LiCl was added to all other solutions and buffered media were used for pH > 1.2. In pH 4.7 and 3 media, two equal, chemically reversible waves are obtained in the potential domains explored (Fig. 10A). In pH 1.2 solution, the two waves observed in pH 3 and 4.7 media undergo a displacement in the positive potential direction and are split; however, the combined peak current intensities remain roughly constant and equal to the intensity of the corresponding original wave at pH 3, for example. The same phenomenon continues at pH 0.3, with a slightly larger splitting and a further move of the whole pattern in the positive potential direction. The behaviour of the first wave as a function of the pH of the solution is shown more clearly in Fig. 10B. Controlled potential coulometry indicates that each of the two waves observed at pH 4.7 or pH 3 corresponds to the consumption of 8 faradays per mole of heteropolyanion. Partic-

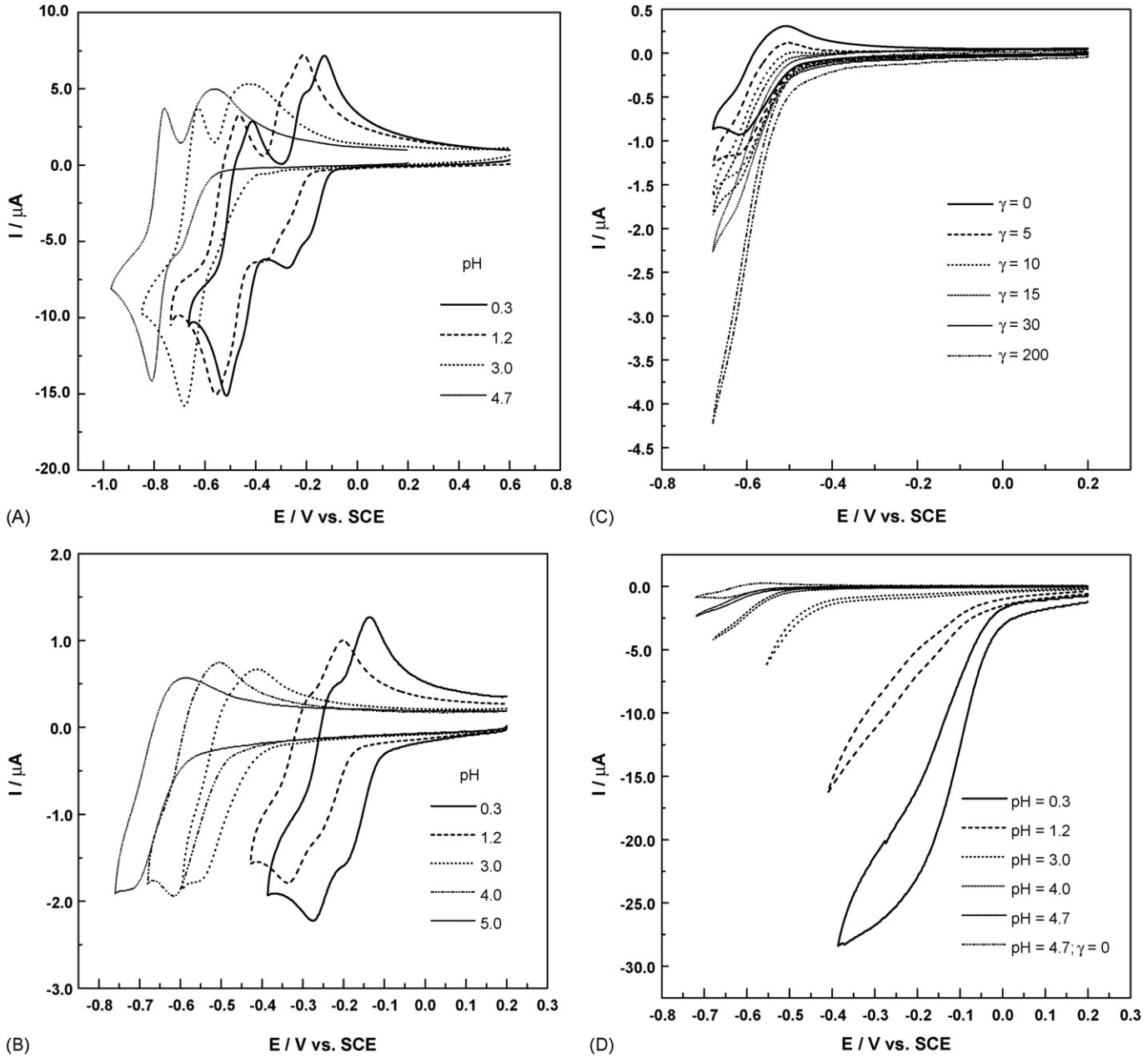

Fig. 10. Evolution of the cyclic voltammograms of P_8W_{48} as a function of the composition of the supporting electrolyte. Scan rate: 10 mV s^{-1}. (A) 5×10^{-4} M P_8W_{48} in various pH solutions: pH 4.7: (0.1 M CH_3COOLi/CH_3COOH + 1M LiCl); pH 3: (H_2SO_4 + 0.069M PHP + 0.5M Li_2SO_4); pH 1.2: (H_2SO_4 + 0.5M Li_2SO_4); pH 0.3: (0.5M H_2SO_4). (B) 10^{-4} M P_8W_{48} in various pH solutions; the study is restricted to the first wave obtained at pH 5 and to its evolution at lower pH values; pH 4 and 5: (0.1M CH_3COOLi/CH_3COOH + 1M LiCl); pH 3: (H_2SO_4 + 0.069M PHP + 0.5M Li_2SO_4); pH 1.2: (H_2SO_4 + 0.5M Li_2SO_4); pH 0.3: (0.5M H_2SO_4). (C and D) Evolution, as probed by cyclic voltammetry, of the catalytic reduction of nitrite observed on the first 8-electron system of 10^{-4} M P_8W_{48}. Scan rate: 2 mV s^{-1}. (C) Evolution as a function of the excess parameter $\gamma = C^{\circ}_{NO_2^-}/C^{\circ}_{HPA}$ in a pH 4 medium (0.1M CH_3COOLi/CH_3COOH + 1M LiCl). (D) Evolution as a function of pH for a constant excess parameter $\gamma = 200$. Electrolyte compositions are the same as those of Fig. 2D. The curve with $\gamma = 0$ pH 4.7 is added for comparison. For further details, see text (taken from Ref. [36]).

ular attention was paid to the first wave at several pH values, in anticipation of its involvement in some catalysis studies. Typically, at pH 1.2, coulometry was carried out on the combined split first wave. The measured consumption was 8.04 faradays per mole of heteropolyanion. After exhaustive electrolysis on this wave, the reduced solution could be reoxidized quantitatively to the initial state at 0 V *versus* SCE. Detailed discussion can be found in the original paper [36].

Fig. 10C shows representative cyclic voltammograms obtained when increasing concentrations of nitrite are introduced in a pH 4 solution of P_8W_{48}. The ratio of the concentration of nitrite to that of the heteropolyanion is designated by $\gamma = c^{\circ}_{NO_2^-}/c^{\circ}_{HPA}$. At this pH, the first 8-electron reduction wave of the oxometalate is not split and the catalytic process is highlighted by the gradual enhancement of the current intensity and the vanishing of the reoxidation trace. For fairly high γ val-

ues, the catalytic wave becomes polarogram-shaped, with the reverse scan current tending to retrace very closely the forward scan current. Correlatively, the plateau current is independent from the scan rate as expected. Fig. 10D displays as a function of pH, the cyclic voltammograms obtained with a constant value of $\gamma = 200$. The catalyst wave at $\gamma = 0$ is added for the sake of comparison. The same general behaviours are observed as at pH 4; however, several details are worth noting. The first 8-electron wave of the oxometalate splits for pH < 3 (*vide supra*) and the catalysis study is then concerned with the whole composite wave. The catalytic pattern moves in the positive potential direction when the pH decreases. It is worth emphasising that the catalytic process proceeds without the presence of a specific transition metal centre to complex the species to be catalyzed. As another step in this study, the problem arises of the identity of the catalyzed species (*vide supra*). For a direct verification, pure NO was bubbled into a pH 1.2 solution of P_8W_{48}. The solubility of NO puts the value of γ at 20. The original reduction pattern of the catalyst is fully restored upon bubbling argon through the NO saturated solution. Even ignoring the slowness of the disproportionation process of nitrite, the observations designate HNO_2 as the main species participating in the catalytic reduction of nitrite in this pH domain. However it was found that the catalytic current in the presence of NO might become strikingly large. In fact, the authors discovered that the catalytic reduction of NO is strongly enhanced by trace amounts of dioxygen in fairly acidic media. Saturation of NO into a pH 1.2/P8W48/air solution gives a catalytic wave, which exceeds by far that observed for NO_2^- with $\gamma = 200$, in the absence of dioxygen. Such observations prompted to study a mixture of nitrite and nitric oxide. A strongly enhanced catalytic wave was obtained compared to those of individual chemicals. Numerous reactions and equilibria among the NO_x [74] in the gas phase and in solution, demand a careful examination before deciding possible species participating in the catalytic processes. Provisionally, it is worth noting that the reaction of NO with molecular dioxygen ends up rapidly in the formation of HNO_2 in solution [74]. Also, the possibility that the reduction of dioxygen is actually being catalyzed is not clearly supported by experimental observations.

Finally, a short comparison with $[P_2Mo_{18}O_{62}]^{6-}$ [10] or $[P_2V_2W_{16}O_{62}]^{8-}$ [28] is in order. From the standpoint of reduction potential, P_8W_{48}, might not seem the best oxometalate for the electrocatalytic reduction of the NO_x. Such a conclusion might be misleading because a much larger number of electrons is involved at this reduction potential, thus giving the possibility to obtain more highly reduced products than N_2O.

4.2. The nature of transition metal center substituent is useful to drive some specific electrocatalytic processes

The first examples of electrocatalytic reduction of nitrate by reduced POMs were obtained with Cu- or Ni-substituted POMs [75]. Specifically, α_2-$P_2W_{15}Mo_2Cu$ was chosen as a representative example to be described in detail.

In its cyclic voltammogram in plain pH 3 electrolyte, Fig. 11A, the copper reduction wave is followed by a third reversible wave attributed to the redox process of the W centres

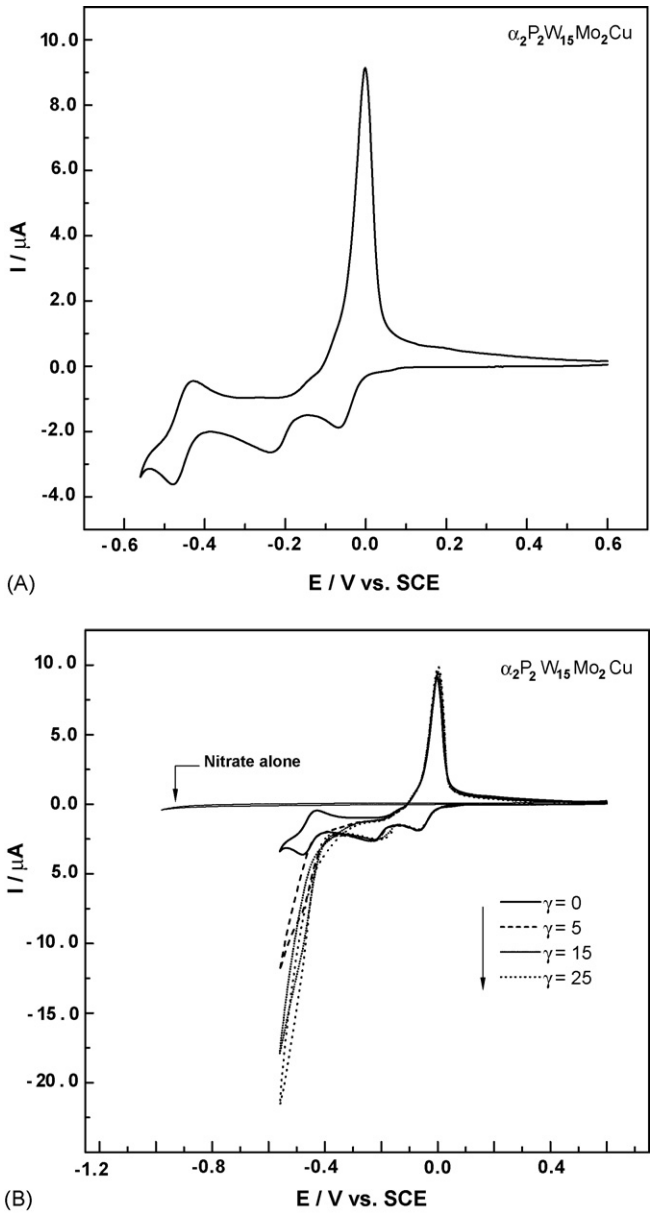

Fig. 11. Cyclic voltammogram restricted to the three first waves of a 5×10^{-4} M solution of α_2-$P_2W_{15}Mo_2Cu$ in 0.2 M $Na_2SO_4 + H_2SO_4$ (pH 3); scan rate: 2 mV s^{-1}; working electrode: glassy carbon. (A) Before and (B) after addition of increasing amounts of nitrate; the excess parameter $\gamma = C^\circ_{NO_3^-}/C^\circ_{HPA}$ is indicated on the figure. For further details, see text (taken from Ref. [75]).

[14,76]. In the presence of increasing concentrations of nitrate, Fig. 11B shows a gradual increase of the reduction current just past the copper reduction wave. Concomitantly, the reversibility of the third wave is suppressed even for small values of the excess parameter γ ($\gamma = C^\circ_{NO_3^-}/C^\circ_{HPA}$). These observations demonstrate the efficient catalysis of nitrate reduction during the reduction of α_2-$P_2W_{15}Mo_2Cu$. It is known that the reduction of nitrate on solid electrodes, including glassy carbon, is a difficult process. Here, it was checked and Fig. 11B shows that no appreciable reduction of nitrate occurs down to −1.0 V in the pH 3 electrolyte in the absence of α_2-$P_2W_{15}Mo_2Cu$. The necessity of copper was easily assessed by carrying out the same

experiments with α_2-$P_2W_{15}Mo_2\square$ (the symbol $\square$ represents the vacancy in the lacunary species) and α_2-$P_2W_{15}Mo_3$. With these two heteropolyanions, no catalysis of the nitrate reduction was observed, even with γ as large as 1000 and potential limits as negative as −0.930 and −0.910 V for the two compounds, respectively, compared to the much less negative limit of −0.560 V for α_2-$P_2W_{15}Mo_2Cu$.

The possible ligand effects were studied by considering the atomic composition of the ligands and the location of the copper centre in the heteropolyanion framework. The following heteropolyanions, were selected: α_1- and α_2-$P_2W_{17}M$, α_1- and α_2-$P_2W_{12}Mo_5M$, α_2-$P_2W_{17}Mo_2M$ and α_2-$P_2W_{13}Mo_4M$ (with M representing any substituent metal center, and, here, specifically Cu^{2+}). The presence of Mo is chosen on purpose [77–80]. From the analysis of the results, it came out that the catalytic properties towards the reduction of nitrate are enhanced by the presence of Mo atoms in the framework. Detailed account of the experiments can be found in the original paper [75]. Various parameters, including the amount of deposited copper, the degree of mixing up of the copper wave with that of another redox center, Mo or W, the morphology of the electroplated film and pH effects were also considered.

However, the following remark, which might limit the importance of these results, made it necessary to compare the behaviours of Cu- and other metal ion-substituted heteropolyanions. As a matter of fact, it can be argued that the foregoing observations replicate merely the catalytic properties known for copper, or eventually of molybdenum, in the electrocatalytic reduction of nitrate ion [77–82].

This comparison was carried out by selecting an extensive series of substituted compounds. Focus is placed more specifically on α_2-$P_2W_{15}Mo_2M$ derivatives (where $M = V^{IV}$, Mn^{II}, Fe^{III}, Co^{II}, Ni^{II}, Cu^{II}, Zn^{II} and) and fully tungstic frameworks, α_1- and α_2-$P_2W_{17}M$ ($M = Co^{II}$, Ni^{II} and Cu^{II}). As previously, the potential scan was restricted to the domain in which the catalysis of proton reduction by heteropolyanions does not occur yet. Among the substituent metal ions, only Fe^{III} and Cu^{II} centres within the heteropolyanions are reduced in this potential domain.

Fig. 12A shows the catalytic reduction of nitrate by α_2-$P_2W_{15}Mo_2Ni$ in a potential regime where no such activity is observed on glassy carbon electrode in its absence. The potential location is clearly more negative than obtained with α_2-$P_2W_{15}Mo_2Cu$; the current intensity is also smaller, even though this parameter should be considered with caution, owing to the possibility of electrode surface area modification upon deposition of copper. A final point of concern will be the comparison of the nature of the product(s) resulting from the two catalytic processes. The comparison in Fig. 12B of two Ni-substituted heteropolyanions is more straightforward than for Cu-substituted molecules, because no deposition process is involved in the electrochemistry of the former. This comparison indicates that the catalytic current for nitrate reduction is the larger with the Mo-containing HPA. Here again, it must be reminded that Mo atoms are in the reduced state and might show a catalytic activity towards the reduction of NO_2^-, if this anion happens to be an intermediate in the catalytic reduction of nitrate, as in the case of Cu-substituted heteropolyanions.

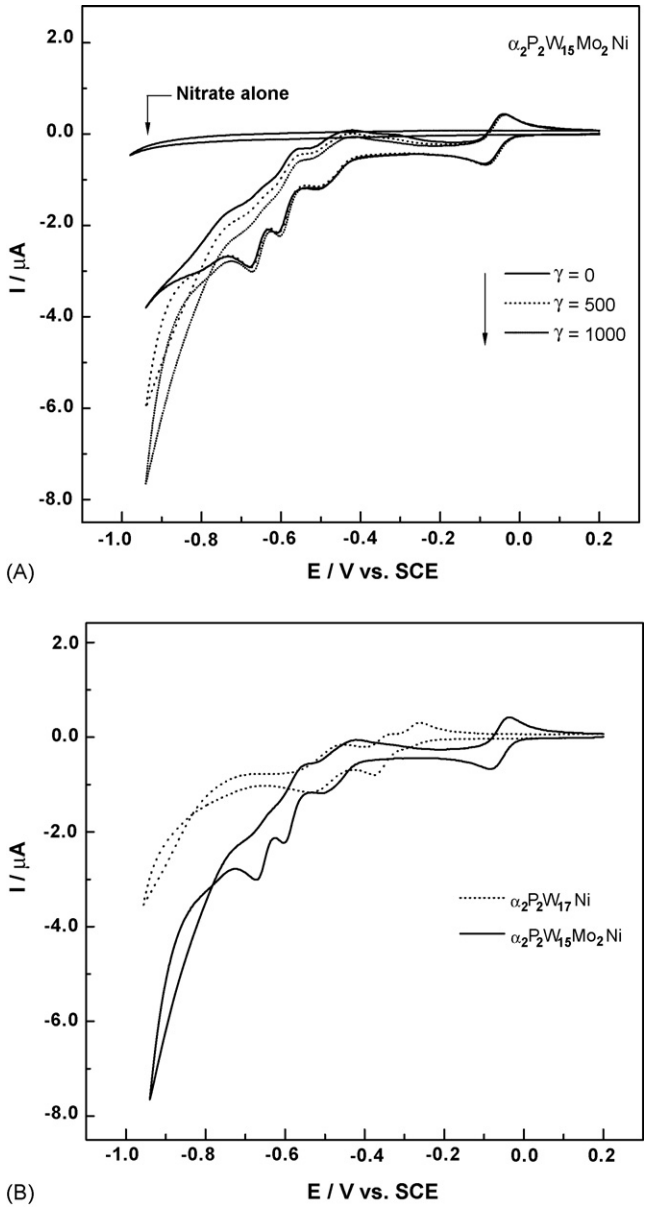

Fig. 12. Cyclic voltammograms of a 2×10^{-4} M solution of α_2-$P_2W_{15}Mo_2Ni$ in 0.2 M $Na_2SO_4 + H_2SO_4$ (pH 3) showing its catalytic activity in the presence of nitrate; scan rate: 2 mV s^{-1}; working electrode: glassy carbon. (A) the excess parameter $\gamma = C^{\circ}_{NO_3^-}/C^{\circ}_{HPA}$ is indicated on each curve. (B) The catalytic activities of α_2-$P_2W_{15}Mo_2Ni$ and α_2-$P_2W_{17}Ni$ are compared for $\gamma = 1000$. For further details, see text (taken from Ref. [75]).

Following these first examples, several confirmations were obtained [75,83–85].

Finally, attempts at catalyzing the reduction of nitrate were performed with all the other heteropolyanions cited above. All the results indicate that these oxometalates are not efficient, at least in the potential domain explored. The cases of α_2-$P_2W_{15}Mo_2M$, α_1- and α_2-$P_2W_{17}M$ derivatives (where $M = Fe^{III}$) deserves particular attention as they indicate that these molecules are not efficient in the electrocatalytic reduction of nitrate. Such an observation complies with the literature where Epstein et al. had shown that efficient oxidation of Fe^{2+} by nitrate

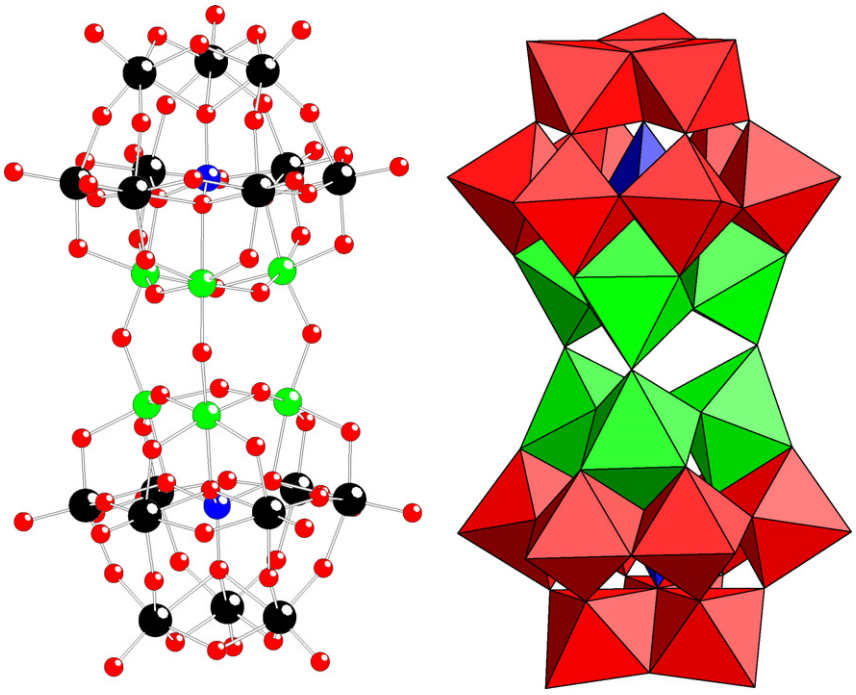

Fig. 13. Ball and stick (left) and polyhedral (right) representations of $[Fe_6(OH)_3(A\text{-}\alpha\text{-}GeW_9O_{34}(OH)_3)_2]^{11-}$. The color code is as follows: iron (green), tungsten (black), germanium (blue) and oxygen (red) (taken from Ref. [87]).

necessitates a catalyst [86]. However, it was discovered recently that the Keggin dimer, $[Fe_6(OH)_3(A\text{-}\alpha\text{-}GeW_9O_{34}(OH)_3)_2]^{11-}$ (abbreviated as $Fe_6Ge_2W_{18}$), with the structure shown in Fig. 13, presents important catalytic activity toward the reduction of nitrate [87]. Fig. 14 indicates that this activity was observed readily when the first W-reduction processes were reached. Furthermore, the potential domain where this electrocatalysis was obtained is comparable with those of the best HPA-based electroacatalysts [85]. Owing to the slightly positive location of the W-wave of $Fe_6Ge_2W_{18}$ relative, for example, to that of $[Ni_4Mn_2P_3W_{24}O_{94}]^{17-}$ [85], the electrocatalytic reduction of nitrate at pH 3 begins roughly 100 mV positive in the case of the former complex. Comparison of the nitrite and nitrate electrocatalysis patterns is enlightening: insofar as nitrite and NO are known to appear as intermediates in the reduction of nitrate on various metals, the potential locations of the corresponding waves would suggest that highly reduced species should be obtained in the electrocatalytic reduction of nitrate in the presence of $Fe_6Ge_2W_{18}$. Provisionally, the remarkable activity of $Fe_6Ge_2W_{18}$ in the electrocatalytic reduction of nitrate is worth emphasizing as it constitutes the first example, to our knowledge, in which such an efficiency is demonstrated for a Fe-containing HPA.

4.2.1. Concluding remarks

The results described in this sub-section reveal unambiguously the importance of the nature of the substituents within the POM framework. Possibly, the location of this substituent or their relative arrangement in case of multiple substitution, should also be taken into account. The example of Ni-substituted POMs within which no electroactivity was detected for the substituent is remarkably enlightening in this respect.

4.3. The number of substituents within the POM framework might influence the catalysis intensity

Separation of the influences of the nature of substituent(s) from that of their number is made for clarity, even though they might mix intimately in several cases. For example, it was found recently [88], that the dimeric pentacopper(II)-substituted tungstosilicate $[Cu_5(OH)_4(H_2O)_2(A\text{-}\alpha\text{-}SiW_9O_{33})_2]^{10-}$ catalyses the reduction of nitrogen protoxide (N_2O). This is probably, the first report of catalysis of this reduction by a POM. In this example and in several others, the nature and the number of substituents might intervene in concert. Keeping specifically first with Cu-substituted POMs, the comparison between the catalytic activities of monosubstituted derivatives with those of sandwich-type complexes had demonstrated the favourable effect of the accumulation of Cu-centers within the same molecule in the electrocatalytic reduction of nitrate [83,84]. Analogous conclusions were reached in the comparison of the efficiencies of Ni-multi-substituted POMs with Ni^{2+}-monosubstituted POMs [85] or Fe^{3+}-sandwich-type POMs with Fe^{3+}-monosubstituted POMs in other reaction processes [87,89].

A particularly striking example is offered by the electrocatalytic behaviours of a new Cu^{2+}-multi-substituted POM [90], containing twenty Cu atoms, $[Cu_{20}Cl(OH)_{24}(H_2O)_{12}(P_8W_{48}O_{184})]^{25-}$ ($Cu_{20}P_8W_{48}$). To our knowledge, this polyanion contains the largest number of 3d transition metal centers among reported polyoxotungstates. This molecule is synthesised from $K_{28}Li_5H_7P_8W_{48}O_{184}\cdot 92H_2O$ (P_8W_{48}) and both compounds were checked to be stable in a large pH domain. Fig. 15 shows the structure of $Cu_{20}P_8W_{48}$. Its electrochemistry was studied in detail [90].

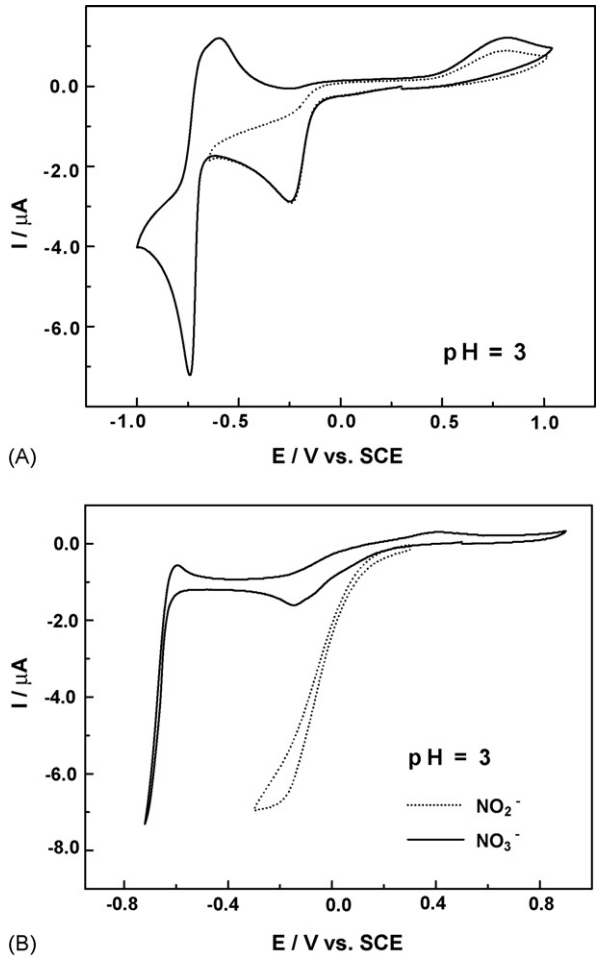

Fig. 14. Cyclic voltammograms in a 2×10^{-4} M solution of 1a in pH 3 media; working electrode: glassy carbon; reference electrode: SCE. (A) pH 3 sulfate medium (0.2 M $Na_2SO_4 + H_2SO_4$); superposition of the CVs restricted to the Fe-wave (dotted line) and to the Fe-wave and the first W-redox processes (continuous line), respectively; scan rate: 10 mV s^{-1}. (B) pH 3 acetate medium (0.4 M $CH_3COONa + ClCH_2COOH$); superposition of the CVs run in the presence of 6×10^{-3} M NO_2^- and 2×10^{-1} M NO_3^-, respectively; scan rate: 2 mV s^{-1} (taken from Ref. [87]).

The polyanion $Cu_{20}P_8W_{48}$ was tested, at pH 0 and 5, for its activity in the reduction of nitrate and the intermediate or final products thereof, namely NO_2^-, HNO_2 or NO. However, only the observations made at pH 5 were described in detail, a medium in which POM-based catalysts are more difficult to obtain than in more acidic solutions. Fig. 16A shows the CVs recorded in the absence and the presence of different concentrations of nitrate. The current is observed to increase readily at the potential location of the first W-wave with increasing nitrate concentration, even for small values of the excess parameter γ (γ is the excess parameter defined here as $\gamma = C^{\circ}_{NO_x}/C^{\circ}_{Cu_{20}P_8W_{48}}$). Concomitantly and beginning from the same small γ values, the W-waves loose their chemical reversibility. For example, the catalytic efficiency CAT varies from 176 to 1088% when γ increases from $\gamma = 10$–60. CAT is defined as $CAT = 100 \times [I_{(HPA+NO_3^-)} - I^d_{(HPA)}]/I^d_{(HPA)}$ where $I_{(HPA+NO_3^-)}$ represents the reduction peak current observed for the heteropolyanion (HPA) in the presence of nitrate and $I^d_{(HPA)}$ is the corresponding reduction peak current for the HPA alone. Provisionally, it is worth noting that the tests carried out at pH 0 show also a large catalytic efficiency for the nitrate reduction with catalytic current intensities larger than those obtained at pH 5, in-line with the dependence of this process on pH. In the two media studied, no direct reduction of nitrate anions on the glassy carbon electrode is observed in the potential domains explored and in the absence of HPA. Using the same conditions, also the ligand P_8W_{48} shows no activity towards this reaction. As a consequence, the presence of copper ions appears to be of utmost importance for observing this catalysis.

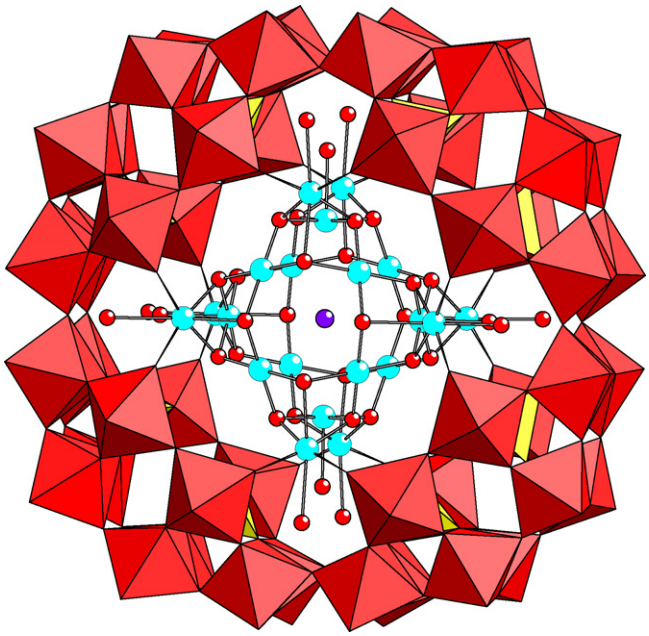

Fig. 15. Combined polyhedral/ball-and-stick representation of $Cu_{20}P_8W_{48}$. The WO_6 octahedra are in red, and the PO_4 tetrahedra are yellow, Cu is turquoise and Cl is violet (taken from Ref. [90]).

The activity of $Cu_{20}P_8W_{48}$ for reductions of NO_2^-, HNO_2 and/or NO was also tested as these species are probable intermediates in nitrate reduction. In addition, another aim was to check the influence of the Cu^{2+} presence, as the pure lacunary ligand P_8W_{48} had been shown to catalyse the reduction of NO_2^-, HNO_2 and NO [36]. Fig. 16B shows the example of nitrite reduction catalysis by $Cu_{20}P_8W_{48}$ at pH 5. This catalysis appears at the potential location of the Cu^{2+}/Cu^+ couple. At pH 0, we have also established that HNO_2 and NO (*vide supra* for the behaviour of $NaNO_2$ in this medium) are efficiently reduced in the presence of $Cu_{20}P_8W_{48}$ at the reduction potential of Cu^{2+}.

Specifically, comparison of $Cu_{20}P_8W_{48}$ and $[Cu_4(H_2O)_2(P_2W_{15}O_{56})_2]^{16-}$ ($Cu_4P_4W_{30}$) is interesting because a twofold aim is achieved with the former complex. As a matter of fact, both the numbers of Cu^{2+} centers and those of W-centers were considerably increased compared to the corresponding ones in $Cu_4P_4W_{30}$. This situation illustrates and justifies the pursued aim to enhance most electrocatalytic processes through intervention of as many as possible fast multi-electron redox couples. For example, in the comparison of $Cu_{20}P_8W_{48}$ and $Cu_4P_4W_{30}$ at pH 5, the number of electrons for W-waves reduction increases from 4 to 8 and that of Cu^{2+}/Cu^+ couple from 4 to 20. For nitrate

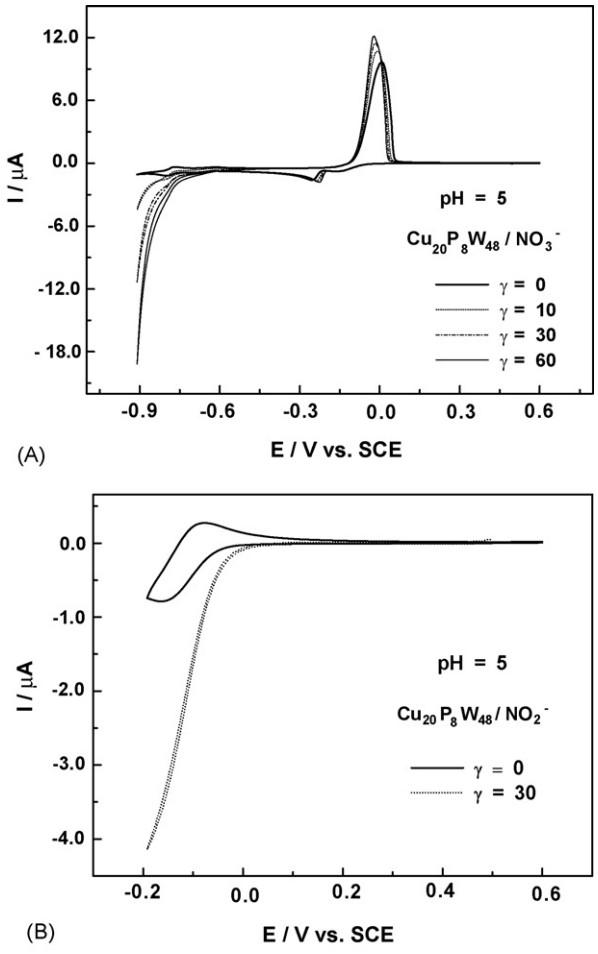

Fig. 16. (A) Cyclic voltammograms (scan rate: $2\,mV\,s^{-1}$) for the electrocatalytic reduction of nitrate with a 4×10^{-5} M solution of $Cu_{20}P_8W_{48}$ in a pH 5 medium (1 M $CH_3COOLi + CH_3COOH$). (B) Cyclic voltammograms (scan rate: $2\,mV\,s^{-1}$) for the electrocatalytic reduction of nitrite with a 4×10^{-5} M solution of $Cu_{20}P_8W_{48}$ in a pH 5 medium (1 M $CH_3COOLi + CH_3COOH$). The excess parameter is defined as $\gamma = C^{\circ}_{NO_x}/C^{\circ}_{Cu_{20}P_8W_{48}}$ (taken from Ref. [90]).

reduction at pH 5, it was found that, in the same experimental conditions and taking into account the number of Cu^{2+} centers, $Cu_{20}P_8W_{48}$ is, for instance, roughly 2.5 times more efficient than $Cu_4P_4W_{30}$ at −0.85 V. At this pH, a potential improvement of roughly 200 mV was observed for the catalytic process, because Cu^{2+} and the catalytically active W-waves are located at more positive potentials in the former complex. The same comparison could not be carried out at pH 0, because $Cu_4P_4W_{30}$ is not stable in this medium, a feature which constitutes an additional advantage of the supermolecular $Cu_{20}P_8W_{48}$ complex.

As concerns nitrite at pH 5, the difference in catalytic efficiencies is still more pronounced: in the same experimental conditions and taking into account the number of Cu^{2+} centers within each complex, $Cu_{20}P_8W_{48}$ is, for example, 3.5 times more efficient than $Cu_4P_4W_{30}$ at −0.19 V. The efficiency, at pH 5, of the pure ligand P_8W_{48} is negligible between 0 and −0.2 V, a domain in which the presence of Cu^{2+} makes $Cu_{20}P_8W_{48}$ show an important catalytic activity. In contrast, the catalysis with the pure ligand is triggered by the W reduction wave located at a much negative potential, at −0.680 V. As a last issue of interest, it should be pointed out that a catalytic effect could be observed with the simple (4×10^{-5} M P_8W_{48} and 8×10^{-4} M $CuSO_4$) mixture. However, for example, in the same measurement conditions, the catalytic efficiency CAT for nitrite reduction by this mixture is 3–11 times smaller than the corresponding value determined for the molecule $Cu_{20}P_8W_{48}$ itself when the pH varies from 5 to 0.

4.3.1. Concluding remark

Finally, it becomes clear that accumulation within the present polyoxometalates of active Cu^{2+} centers is associated with an enhancement of the catalytic properties of this atom, with the supplementary advantage to fabricate highly reduced species with the electrons accumulated in the reduced W framework of the heteropolyanion.

5. Additivity and/or cooperativity of the influences of different metallic centers within the POM framework

This section addresses the observed interactions between two or several metallic centers within POMs, resulting in an overall influence on the homogeneous catalysis of electrode reactions. For clarity and convenience, a distinction is established between POMs substituted in their skeleton by one transition metal center or several such centers and sandwich-type POMs in which the substitution is envisioned in the central metal core.

5.1. Substituted POMs

5.1.1. Cooperativity of Mo- and Cu-centers within POM skeleton for the electrocatalytic reduction of dioxygen and hydrogen peroxide

The electrochemistry of α_2-$P_2W_{15}Mo_2Cu$ is useful in this section and the following one. Fig. 17A shows the part of its cyclic voltammetric pattern of interest in this work. The first two reduction waves were attributed to molybdenum and to copper, respectively [76]. The large desorptive oxidation wave observed during the reoxidation scan features an overlap of the oxidation of the deposited copper with the reoxidation wave of Mo centres. Spectroelectrochemistry experiments at several potentials were useful to help in confirming the attribution of waves. The electrolysis performed at the peak potential of the first wave, (−0.097 V *versus* SCE) is complete after the consumption of 2.1 electrons per molecule [76]. The absorbance of the solution no longer changes upon continuation of the electrolysis at −0.176 V *versus* SCE. It came out that the two-electron reduction of Mo centres in this potential domain is complete before that of the Cu^{II} centre, except for some 5% reduction of the latter. At a more negative potential, roughly two supplementary electrons are used for the reduction of Cu^{2+} into Cu^0. The third wave (not shown) features the reduction of W^{VI} centres.

The main features of the dioxygen electrocatalytic reduction in the presence of α_2-$P_2W_{15}Mo_2Cu$ are illustrated in Fig. 17B by a selection of cyclic voltammograms [91]. The direct reduction of dioxygen on the glassy carbon surface is observed at a fairly negative potential. In contrast, its electrocatalysis occurs readily in the potential domain which was demonstrated previ-

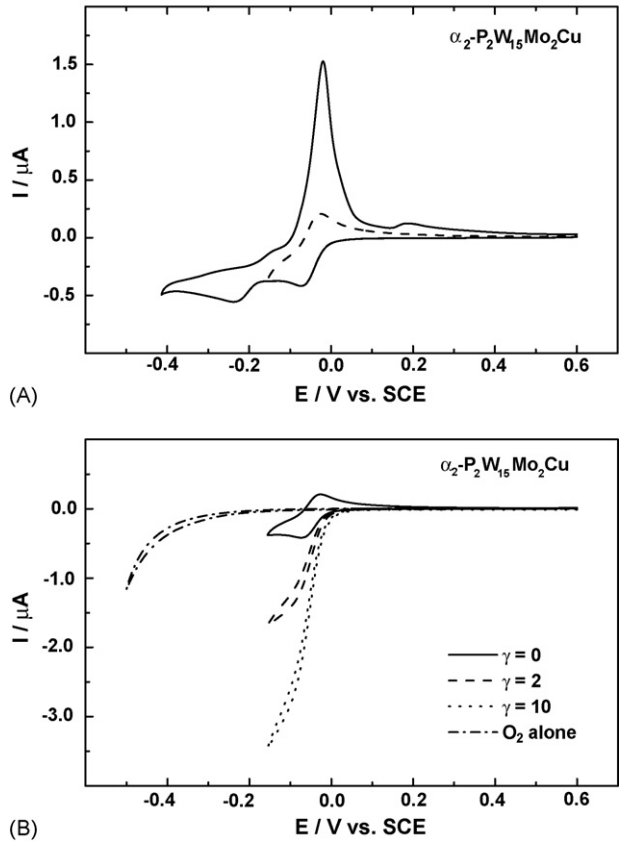

Fig. 17. Cyclic voltammograms (scan rate: $2\,mV\,s^{-1}$) observed in 0.2 M $Na_2SO_4 + H_2SO_4$ (pH 3); working electrode: glassy carbon. (A) 10^{-4} M α_2-$P_2W_{15}Mo_2Cu$. The choice of the reversal potentials helps to distinguish the various steps. (B) dioxygen alone and 10^{-4} M α_2-$P_2W_{15}Mo_2Cu$ in the presence of different concentrations of dioxygen. For further details, see text (taken from Ref. [91]).

ously to correspond mainly to the reduction of Mo centres. It is worth emphasizing that the voltammetric pattern indicates no obvious deposition of copper in this domain. Qualitatively, the efficiency of the catalysis is already revealed even for an excess parameter ($(\gamma = C^{\circ}_{O_2}/C^{\circ}_{HPA})$) as low as $\gamma = 2$. The catalytic efficiency CAT is a useful parameter and is defined as follows: $CAT = 100 \times [I_{(HPA+O_2)} - I^{d}_{(HPA)}]/I^{d}_{(HPA)}$ where $I_{(HPA+O_2)}$ is the peak current for reduction of the heteropolyanion (HPA) in the presence of O_2 and $I^{d}_{(HPA)}$ is the corresponding diffusion peak current for the HPA alone. For $\gamma = 10$, CAT calculated at -0.060 V is 2.5 times larger than for $\gamma = 2$. Whatever the value of γ, the polarogram shape of the cyclic voltammogram at low scan rates must be noted. Also worth of notice is the observation that the plateau current for these polarograms at fixed γ value does not depend on the scan rate. These details facilitate the evaluation of the overall rate constant of the catalytic process [92] which is found to be: $k = 2.1 \times 10^3\ M^{-1}\ s^{-1}$. After completion of the dioxygen reduction experiments, the initial voltammogram under argon was routinely restored by bubbling the inert gas through the solution. This result is taken as an indication that no irreversible complex was formed between dioxygen and the oxidized HPA. At slow scan rate, the electrocatalytic activity is also observed on the other waves beyond the first one. A correct comparison with the activity of a solution of pure copper sulphate is plagued or, at least, made difficult by several parameters: the difference in diffusion coefficient between the HPA and Cu^{2+}; some deposition of copper modifying the electrode surface area; the potential at which the catalysis begins, etc. Nonetheless, even ignoring these shortcomings, the catalytic efficiency of the HPA was found to remain better than that of Cu^{2+} alone. Two complementary results must be noted: (i) pH effects were studied; (ii) hydrogen peroxide was found to be reduced in the same potential domain as dioxygen; (iii) water was demonstrated to be the final product of the reduction of dioxygen in the present conditions.

The closeness of the reduction potentials of Mo and Cu centres within the molecule of α_2-$P_2W_{15}Mo_2Cu$ at most pH values, where the catalysis occurs, raises the question of the actual role of each particular atom in the electrocatalytic reduction of dioxygen. Various parameters of the system were studied to clarify the situation. In Fig. 18A are compared the catalytic activities of α_2-$P_2W_{15}Mo_2Cu$ and its lacunary precursor α_2-$P_2W_{15}Mo_2\square$, where the symbol $\square$ represents the vacancy. It is worth noting that the Mo centres are reduced at the same potential in both the lacunary and the Cu-substituted complexes. The lacunary heteropolyanion develops no dioxygen reduction

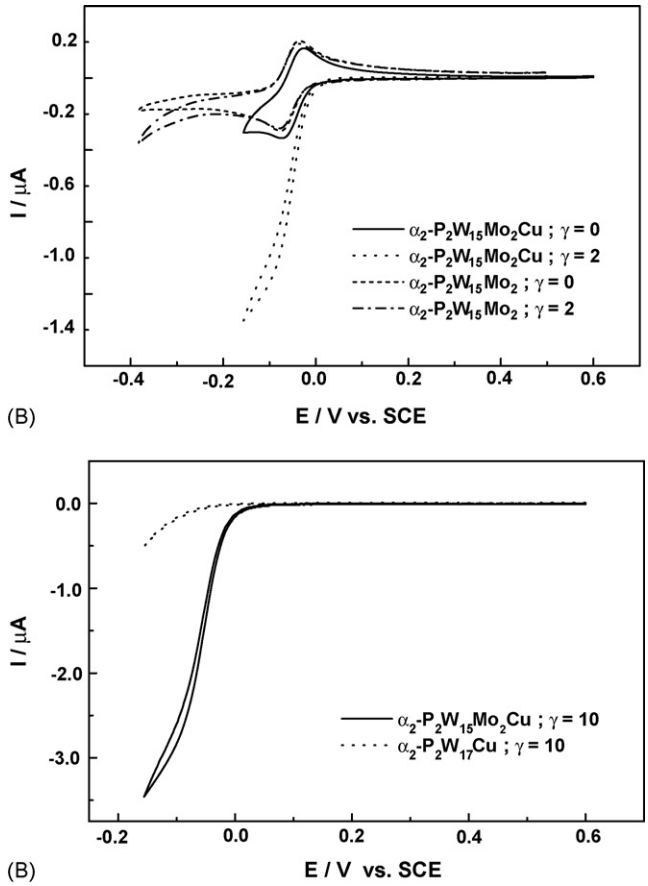

Fig. 18. Cyclic voltammograms (scan rate: $2\,mV\,s^{-1}$) observed in 0.2 M $Na_2SO_4 + H_2SO_4$ (pH 3); working electrode: glassy carbon. (A) Comparison of the behaviours of 10^{-4} M α_2-$P_2W_{15}Mo_2$ and 10^{-4} M α_2-$P_2W_{15}Mo_2Cu$ in the absence and in the presence of dioxygen. For further details, see text. (B) Comparison of the behaviours of 10^{-4} M α_2-$P_2W_{17}Cu$ and 10^{-4} M α_2-$P_2W_{15}Mo_2Cu$ in the presence of dioxygen. For further details, see text (taken from Ref. [91]).

catalysis in the potential domain of reduction of Mo moieties. Indeed, a catalytic effect is seen to start at the substantially more negative potential corresponding to the first reduction wave of W centres. Provisionally, it is worth noting that such catalysis of the dioxygen reduction on the W waves is encountered in most of the heteropolyanions studied to-date. Keeping specifically with the Mo atom, it was found also that the first wave of α_2-$P_2W_{15}Mo_3$ does not show any catalytic activity toward dioxygen, even though sufficiently energetic electrons are available. It must be concluded, at the very least, that the Mo centres alone within α_2-$P_2W_{15}Mo_2Cu$ are not the loci of the observed catalysis process.

α_2-$P_2W_{17}Cu$ was selected to test and compare the catalytic ability of another closely related Cu-containing heteropolyanion in the dioxygen electrocatalytic reduction. Its electrochemistry at pH 3 was studied previously [76]. Its first wave was observed at a more negative potential than the Mo-wave of α_2-$P_2W_{15}Mo_2Cu$. Copper deposition during the first reduction wave of α_2-$P_2W_{17}Cu$ was revealed by the characteristic stripping oxidation wave on potential reversal [76]. In this compound, the first W wave was shown to overlap partly with the copper wave. Spectroelectrochemistry studies indicated, however, that the two-electron reduction of Cu^{2+} is complete before any significant reduction of W moieties.

In the present work, the electrocatalytic dioxygen reduction by reduced α_2-$P_2W_{17}Cu$ is indeed observed (not shown). In contrast with the case of α_2-$P_2W_{15}Mo_2Cu$, the catalytic wave current intensity depends on the scan rate. The characteristic stripping oxidation wave of the copper deposited during the cathodic processes diminishes drastically upon increase of the γ values. All these observations together point to a prominent role of the copper centre within α_2-$P_2W_{17}Cu$ in the catalytic reduction of dioxygen, albeit at a substantially more negative potential than observed with α_2-$P_2W_{15}Mo_2Cu$.

Fig. 18B compares the currents of the catalytic waves obtained in identical experimental conditions with α_2-$P_2W_{15}Mo_2Cu$ and α_2-$P_2W_{17}Cu$, respectively. The electrocatalytic process is less favourable with the latter complex, in which the catalysis can be admitted to be triggered essentially by the Cu center. In other words, no synergism could be observed between the W and Cu influences in the explored potential domain. In contrast, this result, associated with the lack of "intrinsic" activity of Mo centers, highlights the cooperativity between Mo and Cu centres within α_2-$P_2W_{15}Mo_2Cu$ in the electrocatalytic dioxygen reduction.

The question arises as to the actual sequence of events that end up in the reduction of dioxygen into water. Several observations are worth mentioning provisionally. The reoxidation of reduced POMs by dioxygen after the catalytic processes in which they participate is a popular practice. Its mechanism was generally and indistinctly explained to go through an intermediate adduct formation accompanied by inner sphere electron transfers [93]. This and related processes have received further insight recently. Duncan and Hill [94a] established clearly that simple outer sphere electron transfer might be the actual pathway in the case of unsubstituted POMs; in the case of vanadium-substituted derivatives, the conclusion was less clear-cut. The work of Duncan and Hill with isotopic labels does establish that POM oxygens are lost during POM reduction and subsequent reduction of O_2 (reduced POM re-oxidation). In addition, Neumann et al. showed that the some molybdates do lose oxygens upon reduction and these are replenished by other oxygen sources upon reoxidation, thus following a Mars van Krevelen-type mechanism [94b]. The present results should be considered in the framework of metal ion-substituted complexes. In other words, the reasoning should parallel those used in the dioxygen electroreduction by copper-containing organometallic complexes. In these examples, "Cu(I)-O_2" constitutes the favourite intermediate [95]. Here, the proximity of the reduction potentials of Mo and Cu^{2+} centres within α_2-$P_2W_{15}Mo_2Cu$ at appropriately selected pH values suggests strongly that such a mechanism could be operative. Furthermore, the efficiency of the catalysis would indicate that the reduction potential of the adduct is very close to or even more positive than that of Mo centres. Tentatively, mixed acceptor orbitals containing both Mo and Cu contributions can be suggested to exist.

Finally, the possibility that a specificity of the Mo/Cu association exists to favour the observed cooperativity should be considered. Even though the present results were obtained in homogeneous conditions, a parallel can be, tentatively, made with the case of catalytic solid electrodes prepared for the reduction of dioxygen into water: specifically, $(Ru_{1-x}Mo_x)_ySeO_z$ layers containing very small amounts of Mo realise the four-electron reduction of dioxygen in acidic media [96]. The presence of Mo was demonstrated to be required to favour the catalytic process. The mechanistic assumption which guided to the synthesis and study of such layers is that oxygen is adsorbed by Mo due to its higher interaction energy among the surface atoms, but the electrocatalysis must occur at the ruthenium. Such cooperativity can be considered as a successful operational hypothesis.

5.1.2. Facilitation of NO_x reduction by the presence of molybdenum in Fe- or Cu-substituted heteropolytungstates

Several Fe- and Cu-containing Wells–Dawson type tungtodiphosphates substituted by two, four or five Mo atoms are studied by cyclic voltammetry at pH 3 and 5. The following heteropolyanions were selected and synthesised [13b,97]: α_2-$K_8[Cu(OH_2)P_2W_{15}Mo_2O_{61}]$ (abbreviated as α_2-$P_2W_{15}Mo_2Cu$) and α_2-$K_7[Fe(OH_2)P_2W_{15}Mo_2O_{61}]$ (abbreviated as α_2-$P_2W_{15}Mo_2Fe$) and α_2-$K_7[Fe(OH_2)P_2W_{12}Mo_5O_{61}]$ (abbreviated as α_2-$P_2W_{12}Mo_5Fe$) and α_2-$K_7[Fe(OH_2)P_2W_{13}Mo_4O_{61}]$ (abbreviated as α_2-$P_2W_{13}Mo_4Fe$); α_1 and α_2-$K_8[Cu(OH_2)P_2W_{12}Mo_5O_{61}]$ (abbreviated as α_1- and α_2-$P_2W_{12}Mo_5Cu$) and α_2-$K_8[Cu(OH_2)P_2W_{13}Mo_4O_{61}]$ (abbreviated as α_2-$P_2W_{13}Mo_4Cu$). Their main electrochemical characteristics are gathered on Table 6. This electrochemistry was found to depend critically on the pH of the supporting electrolyte, on the number of molybdenum atoms in the POM skeleton and on the location of the Fe- or Cu-substituent in this framework. For example, in a pH 3 medium the first wave of α_2-$P_2W_{15}Mo_2Fe$ features an overall three electron process, in contrast with the well-separated Fe-centered and W-centered processes in α_2-$P_2W_{17}Fe$. In the same medium, the first Mo-wave is observed at a fairly positive potential and precedes the

Table 6
Main reduction peak potentials at pH 3 and 5 for the (Fe or Cu)-substituted molybdo-tungstodiphosphates studied in this work

Heteropolyanion	pH	$-E_{pc}$ (mV)		
		Mo wave	Fe or Cu wave	First W wave
$\alpha_2P_2W_{13}Mo_4Fe$	3	−176	68	320
$\alpha_2P_2W_{13}Mo_4Fe$	5	−46	234	482
$\alpha_2P_2W_{12}Mo_5Fe$	3	−158	48	208
$\alpha_2P_2W_{12}Mo_5Fe$	5	−34	242	360
$\alpha_2P_2W_{15}Mo_2Cu$	3	66	180	476
$\alpha_2P_2W_{13}Mo_4Cu$	3	−144	174	318
$\alpha_2P_2W_{12}Mo_5Cu$	3	−116	198[a]	–

Potential values were culled from the cyclic voltammograms run at a scan rate of 2 mV s^{-1}. Reference electrode: SCE (taken from Ref. [97]).
[a] Merging of the Cu and W waves.

Fe-centered wave for α_2-$P_2W_{13}Mo_4Fe$ and α_2-$P_2W_{12}Mo_5Fe$. In the evaluation of these POMs in the electrocatalytic reduction of nitrite, a nitrosyl complex is formed in a first step. A further reduction of this complex is obtained readily in the cases of α_1-$P_2W_{17}Fe$ and α_2-$P_2W_{15}Mo_2Fe$. Provisionally, it must be noted that the Fe- and the first W-process are fairly well merged for α_1-$P_2W_{17}Fe$ in this medium. The better efficiency of α_2-$P_2W_{15}Mo_2Fe$ is expressed through a more positive peak potential for the relevant wave and a larger peak current intensity.

For α_2-$P_2W_{13}Mo_4Fe$ and α_2-$P_2W_{12}Mo_5Fe$ in which the possibility of merging of waves is now lost, no appreciable catalytic activity towards nitrite was observed at the potential of the well separated Mo-wave. The catalytic process is actually observed to start just past the peak potential of the third wave. This inefficiency was associated, at least in part, with the loss in cooperativity between Mo and Fe centres within the molecule. In any case, the potential locations indicate that α_1-$P_2W_{17}Fe$ and α_2-$P_2W_{15}Mo_2Fe$ are better catalysts than α_2-$P_2W_{13}Mo_4Fe$ and α_2-$P_2W_{12}Mo_5Fe$ at pH 3, probably owing to the merging possibilities of their relevant waves in the former complexes.

Closely related phenomena were observed in the electrocatalytic reduction of nitrite and nitrate by reduced α_2-$P_2W_{15}Mo_2Cu$ [13b,97]. The first wave for this molecule was shown to feature the reduction of the Mo centres in this molecule, without any interference from the reduction of the Cu: such a conclusion stems from preparative scale electrolysis coupled with UV–visible spectroscopy. Fig. 19 describes the phenomena for nitrite reduction at pH 3. In this figure, the curve for $\gamma = 0$ shows no deposition of copper in the potential domain explored, in agreement with known results. Several verifications were carried out. It was checked that copper deposition from $CuSO_4$ solutions commences in the same potential domain and in the absence of nitrite. It was also confirmed that copper electrodeposited from a $CuSO_4$ solution reduces nitrite. Turning to the curves for $\gamma = 10$, it is observed in Fig. 19 that the catalytic reduction of nitrite starts readily on the first reduction wave of α_2-$P_2W_{15}Mo_2Cu$. Then, the interference of copper in this process, if any, is not obvious, and one must look for complementary experimental indications. An interesting observation was made in the following way: the potential domain for the

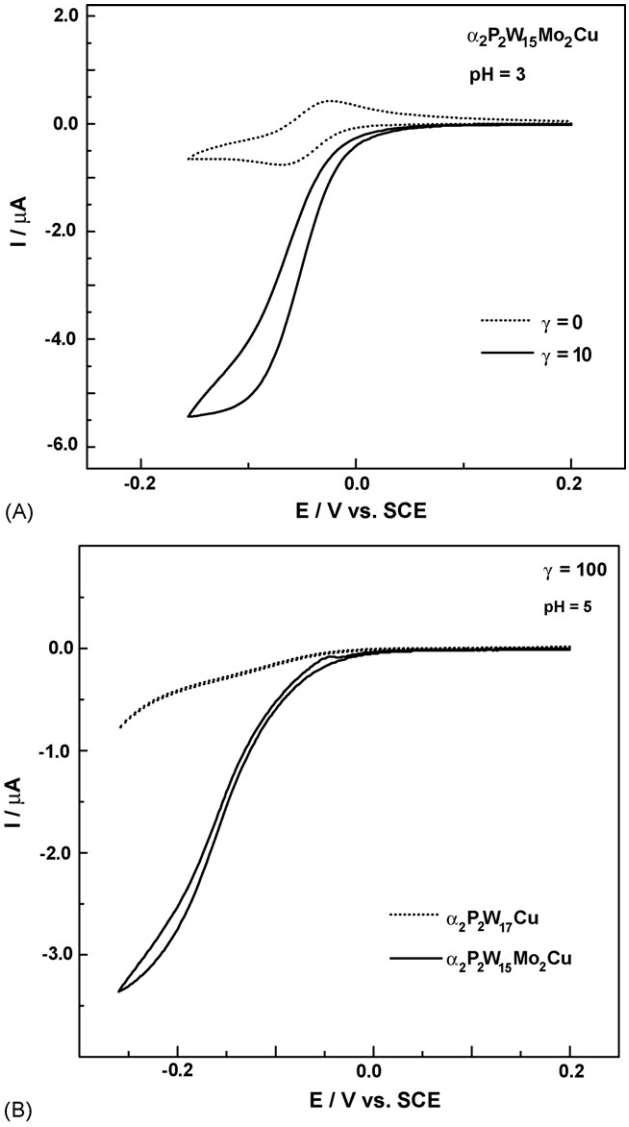

Fig. 19. Cyclic voltammograms observed for 2×10^{-4} M solution of Cu-substituted POMs and showing their catalytic activity in the presence of nitrite; scan rate: 2 mV s^{-1}. The formula of the copper salt, the abbreviated formula of the oxometalate and the pH of the solution are indicated on the figures. (A) Comparison of cyclic voltammograms of α_2-$P_2W_{15}Mo_2Cu$ in the absence and presence of an excess $\gamma = 10$ of nitrite. (B) Comparison of the catalytic activities of α_2-$P_2W_{17}Cu$ and α_2-$P_2W_{15}Mo_2Cu$ in the presence of an excess $\gamma = 100$ of nitrite. For further details, see text (taken from Ref. [97]).

study of the catalysis by α_2-$P_2W_{15}Mo_2Cu$ was extended so that a large electrodeposition of copper could be expected. Then, for $\gamma = 10$ an important decrease in the copper reoxidation wave after the catalytic process was observed. This copper reoxidation wave vanishes completely when γ is further increased. Furthermore, the value of current intensity in the potential domain explored in Fig. 17 shows that no appreciable electrode surface area increase can be invoked. Complementary comparison was carried out with α_2-$P_2W_{15}Mo_3$. Despite a larger number of Mo atoms in the skeleton of this HPA compared to α_2-$P_2W_{15}Mo_2Cu$, the first several waves of $P_2W_{15}Mo_3$ are hardly catalytic towards nitrite. Furthermore, irrespective of stability problems, α_2-$P_2W_{15}Mo_2\square$ appeared as the weakest catalyst (the

symbol □ represents the vacancy in the lacunary species). All these observations together were traced to the two following reasons: the charge consumed during the cathodic scan is shared for the reduction of the Mo and Cu centres; Cu participates as a redox reagent in the reduction of nitrite. Finally, an interaction between copper and nitrite can be hypothesized to explain the observed phenomena, even though no direct experimental evidence for the reduction of copper was obtained. In short, such a behaviour would suggest a beneficial cooperation of the copper and molybdenum centres in α_2-$P_2W_{15}Mo_2Cu$. These observations underscore the favourable role of the presence of copper in the molecule. Finally, Fig. 19B compares the catalytic activities toward the reduction of nitrite of α_2-$P_2W_{17}Cu$ and α_2-$P_2W_{15}Mo_2Cu$. The superiority of the Mo derivative does not call for further comments.

5.2. Sandwich-type POMs

There are five major families of sandwich POMs, four of which are derived from trivacant Keggin structures. In the following, illustrations are carried out mainly with members of the fifth family, consisting of the Wells–Dawson-derived structures. These complexes are composed of a central M_4O_{16} unit encapsulated by two B-α-$[X_2W_{15}O_{56}]^{12-}$ ($X = P^V$ or As^V) trivacant POMs. The selected POMs include αββα-$Na_{12}(Fe^{III}OH_2)_2(Fe^{III})_2(As_2W_{15}O_{56})_2$ (Fe_4As_4), αββα-$Na_{12}(Fe^{III}OH_2)_2(Fe^{III})_2(P_2W_{15}O_{56})_2$ (Fe_4P_4), αααα-$Na_{16}(NaOH_2)_2(Fe^{III})_2(X_2W_{15}O_{56})_2$ (X = As(V) (Fe_2As_4) or P(V) (Fe_2P_4)), ααβα-$Na_{14}(NaOH_2)(Fe^{III}OH_2)(Fe^{III})_2(X_2W_{15}O_{56})_2$ (X = As(V) (Fe_3As_4) or P(V) (Fe_3P_4)) and the mixed-metal complexes, αββα-$Na_{14}(Mn^{II}OH_2)_2(Fe^{III})_2(X_2W_{15}O_{56})_2$ (X = As(V) ($Mn_2Fe_2As_4$) or P(V) ($Mn_2Fe_2P_4$). Their structure are sketched in Fig. 20. In the pH 3 medium (2 M NaCl + HCl) to be used in catalysis studies, their electrochemistry is dominated by the stepwise reduction of the Fe-centers. Fig. 21 shows, in superposition, the voltammograms of Fe_4As_4, Fe_3As_4, and Fe_2As_4, restricted to the waves attributed to the reductions of the Fe(III) centers only. Several conclusions emerge from these patterns. For each CV, the number of waves corresponds to the number of Fe(III) atoms in each complex. These observations suggest there are sufficiently strong interactions between the Fe(III) centers in each of the complexes to induce complete splitting of their redox processes into separate steps. Qualitatively, the overall current intensities are also consistent with the number of Fe(III) atoms in each complex. The number of Fe(III) centers was also checked by controlled potential coulometry measurements, which give three electrons per molecule for Fe_3As_4 and Fe_3P_4 and two electrons per molecule for Fe_2As_4 and Fe_2P_4 for the exhaustive reduction of these centers. At pH 3, the following values were determined: 3.95 ± 0.05 electrons per molecule for Fe_4As_4 and Fe_4P_4 at −0.250 V (*versus* SCE); 2.95 ± 0.06 electrons per molecule for Fe_3As_4 and Fe_3P_4 with the potential set at −0.300 V (*versus* SCE); 1.95 ± 0.07 electrons per molecule for Fe_2As_4 and Fe_2P_4 at −0.360 V (*versus* SCE). The CV patterns shift in the negative potential direction with a decrease in the number of Fe(III) atoms. This is most likely related to the overall increase in the negative charge of the POM due to the decrease in the number of Fe(III) atoms. It is probably also related to pK_a differences in the reduced forms. Further details can be found in the original papers [98,99].

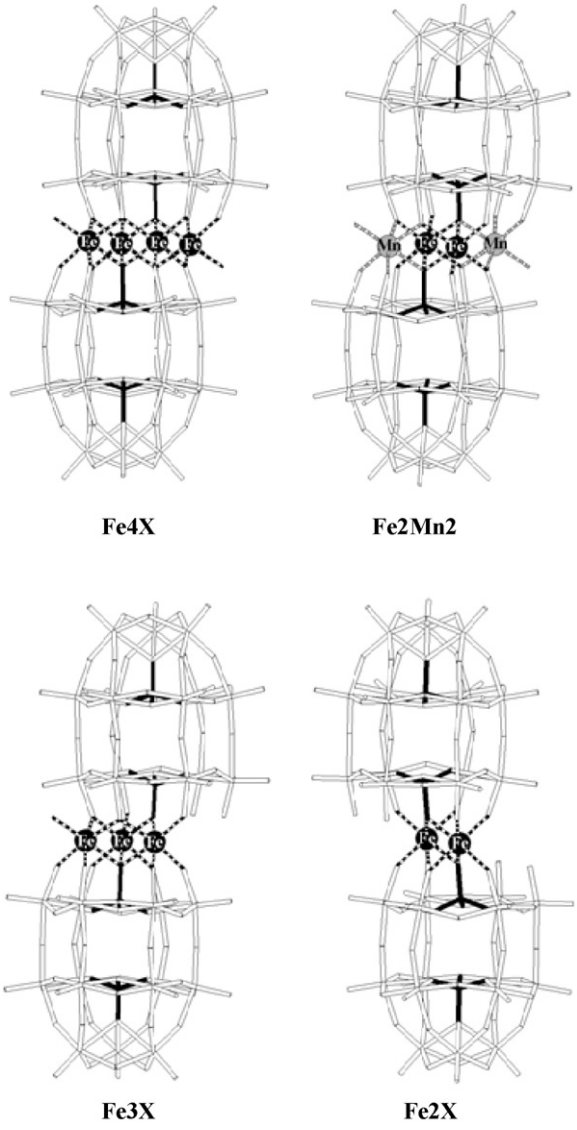

Fig. 20. Combination wireframe/ball-and-stick representations of the eight multi-iron Wells–Dawson sandwich-type complexes studied in this manuscript (taken from Ref. [99]).

Mixed metal sandwich-type complexes are also of prime importance in the present issue. In addition of ($Mn_2Fe_2As_4$) or ($Mn_2Fe_2P_4$) already cited in this section [98,99], electrocatalytic reaction were also studied for αββα-$[(Zn^{II}OH_2)_2(Fe^{III})_2(P_2W_{15}O_{56})_2]^{14-}$ ($Zn_2Fe_2P_4$) and αββα-$[(Zn^{II}OH_2)_2(Fe^{III})_2(As_2W_{15}O_{56})_2]^{14-}$ ($Zn_2Fe_2As_4$) [62] and for the banana-shaped $[Ni_4Mn_2(H_2O)_2P_3W_{24}O_{94}]^{17-}$ [100]. This last complex proved efficient for the reduction of the NO_x. Keeping, for clarity, with Fe_xX_4 (X = P or As; $x = 2, 3, 4$), their useful electrochemistry in the present issue is restricted to Fe-waves and was described in detail in the original papers [62,98,99].

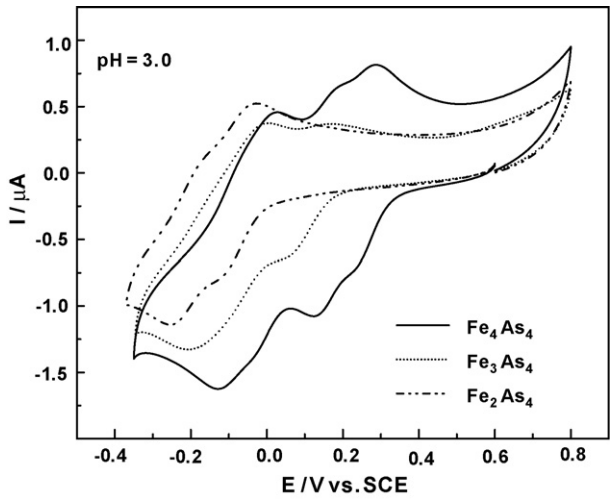

Fig. 21. Cyclic voltammograms of Fe_4As_4, Fe_3As_4, and Fe_2As_4 in 2×10^{-4} M, pH 3 (2 M NaCl + HCl) buffer solution. The scan rate was 10 mV s^{-1}, the working electrode was glassy carbon, and the reference electrode was SCE (taken from Ref. [99]).

5.2.1. Cooperative effects in the electrocatalytic reduction of dioxygen and hydrogen peroxide

Fe_xX_4 (X = P or As; x = 2, 3, 4) complexes are selected for this study. A pH 3 medium was selected for the studies of the electrocatalytic reductions of O_2 and H_2O_2. The efficiency of the catalysis is evaluated by a excess parameter γ, which is defined as $C^{\circ}_{O_2}/C^{\circ}_{POM}$ for dioxygen and $C^{\circ}_{H_2O_2}/C^{\circ}_{POM}$ for hydrogen peroxide (C° = concentration of the relevant species indicated as a suffix) [91 or *vide supra*]. The catalytic efficiency (CAT) is defined as follows: $CAT = [I(POM + O_2 \text{ or } H_2O_2) - I^d(POM)]/I^d(POM)$, where $I(POM + O_2 \text{ or } H_2O_2)$ is the current for the reduction of the POM in the presence of O_2 or H_2O_2 and I^d is the corresponding diffusion current for the POM alone.

Fig. 22A shows the CVs for Fe_4As_4 in the absence and presence of dioxygen. The electrocatalytic reduction of O_2 starts after the second Fe(III) wave and precludes the possibility of observing any other Fe(III) reduction waves. This is consistent with the formation of an iron-dioxygen adduct upon reduction of the first two Fe(III) centers. This adduct is subsequently reduced to give water with regeneration of the catalyst. An inner sphere mechanism is likely operating. Water was confirmed to be the final product in the hydrogen peroxide reduction studies by the same catalytic system. It is interesting that the final reduction process starts past the second Fe(III) wave. Since the naked electrode does not reduce dioxygen in the potential domain explored here, then electrocatalysis must be driven by the reduced forms of the POM [33]. At the potential location of the second Fe(III) wave, the number of electrons accumulated in the POM framework is not sufficient to carry out the overall process. Fig. 22B

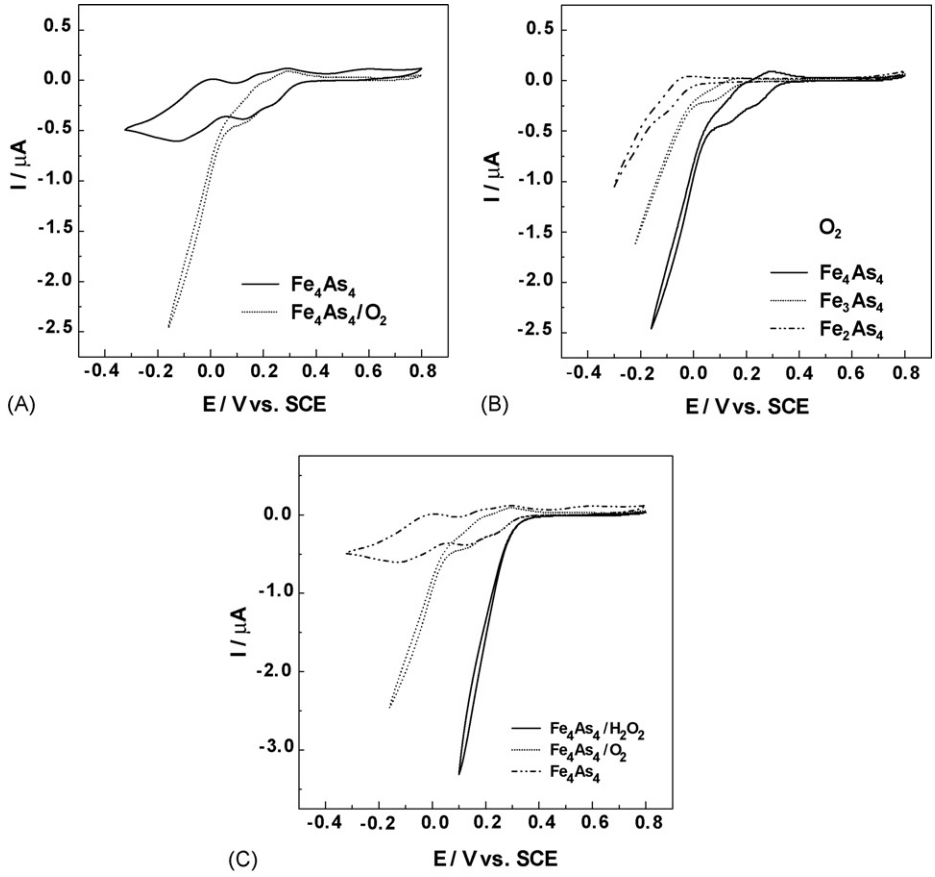

Fig. 22. Cyclic voltammograms for the electrocatalytic reduction of dioxygen and hydrogen peroxide. The excess parameter for dioxygen or hydrogen peroxide was γ = 5, the scan rate was 2 mV s^{-1}, the working electrode was glassy carbon, the reference electrode was SCE, the concentration of the POM was 2×10^{-4} M, and the buffer was pH 3 (2 M NaCl + HCl). (A) Electrocatalytic reduction with Fe_4As_4; (B) Comparison of Fe_4As_4, Fe_3As_4, and Fe_2As_4; (C) Comparison of the catalytic activity of Fe_4As_4 towards dioxygen and hydrogen peroxide reduction (taken from Ref. [99]).

compares the CVs of Fe_4As_4, Fe_3As_4, and Fe_2As_4 in the presence of the same excess of dioxygen. The onset of the electrocatalytic process shifts in the negative potential direction when the number of Fe(III) atoms decreases. Qualitatively, the catalytic efficiency follows the same trend. The preceding reasoning postulating an overall inner sphere process remains valid here, even though an obvious binding site for dioxygen on Fe_2As_4 is difficult to designate.

The electrocatalytic reduction of hydrogen peroxide by Fe_4As_4 is shown in Fig. 22C and compared with the reduction of dioxygen by the same system. The catalytic reduction of H_2O_2 is facile on the first Fe(III) wave of Fe_4As_4 at a potential much more positive than observed for the electrocatalytic reduction of O_2. This observation indicates that the final reduction product of dioxygen is water. Complexes Fe_2As_4 and Fe_3As_4 give similar results, and the onset of the electrocatalytic process is seen to strictly follow the order of reduction of the three complexes.

Selected values of catalytic efficiencies (CAT) for the reduction of dioxygen and hydrogen peroxide are included in Table 7. The general trends from Fig. 22 are confirmed and quantified. Focusing specifically on complexes Fe_4As_4 and Fe_4P_4, it appears that, under the same experimental conditions, the phosphorus-containing complex, Fe_4P_4, is slightly more efficient than the arsenic analogue, Fe_4As_4, for dioxygen reduction, while the opposite is true for hydrogen peroxide reduction. This observation underscores the impossibility to anticipate which electrocatalyst would be the more efficient when an inner sphere pathway is operative. Provisionally, it appears that the same trend was obtained in CAT values for $M_2Fe_2X_4$ (X = P or As; M = Zn(II) or Mn(II)) [62]. Three points deserve special emphasis. First, the electrocatalytic processes observed here remain efficient in other media. For example, at pH 5, a CAT value of 523% was measured for the electrocatalytic reduction of O_2 by Fe_4P_4 at a potential of −240 mV. This observation and others not specifically described here are important in that they establish the utility of the Fe(III) centers within these multi-iron sandwich complexes in media of low proton availability. Second, ample room might still exist for optimization of the selected media for efficient electrocatalytic processes within these compounds. Third, despite the apparent superiority of Fe_4As_4 and Fe_4P_4 in the present voltammetric study, Fe_3As_4 and Fe_3P_4 might ultimately be the most useful long term catalysts, in part due to their better stability over a wide range of conditions [97,101].

Examination of these two electrocatalytic processes sheds some light on the reaction pathways. Dioxygen does not coordinate to Fe(III) but it does coordinate to Fe(II). In the presence of only one Fe center (as in α_2-$As_2(FeOH_2)W_{17}O_{61}^{7-}$), no electron source is available just past the reduction potential of Fe(III) to drive the catalytic process to completion. This observation underscores the importance of the accumulation of Fe(III) centers which carry out immediate further reduction of the adduct. Also noteworthy is that the accumulation of these catalytic centers diminishes the overall negative charge of the POM, rendering its reduction more facile, and ultimately, saving energy during the electrocatalytic process. If complexation of the Fe(III) centers is possible with H_2O_2, then this might constitute a favorable process for its electrocatalytic reaction. In support of this, complexes Fe_3As_4 and Fe_3P_4, which have only one such exchangeable center, have roughly the same efficiency as α_2-$As_2(FeOH_2)W_{17}O_{61}^{7-}$ for the electrocatalytic reduction of H_2O_2.

Analogously, Fe_4As_4 was compared to α_2-$[As_2(Fe^{III}OH_2)W_{17}O_{61}]^{7-}$ and found to be a more efficient catalyst for the reduction of dioxygen [89].

In short, the superiority observed in cyclic voltammetry for tetraferric over triferric and diferric complexes in the electrocatalytic reduction of dioxygen and hydrogen peroxide might be traced, at least partly, to the communication between the metal centers of the respective central cores of these POMs [62,89,98,99].

Table 7
Selected values of catalytic efficiencies measured at pH 3 (2 M NaCl + HCl) for O_2 and H_2O_2 reductions (taken from the SI of Ref. [99])

HPA	CAT% for O_2 reduction	CAT% for H_2O_2 reduction
Fe_4P_4	366 (at −160 mV)	731 (at 66 mV)
Fe_4As_4	313 (at −160 mV)	867 (at 66 mV)
Fe_3P_4	364 (at −220 mV)	546 (at 16 mV)
Fe_3As_4	237 (at −220 mV)	619 (at 16 mV)
Fe_2P_4	217 (at −300 mV)	214 (at −160 mV)
Fe_2As_4	189 (at −300 mV)	233 (at −160 mV)

5.2.2. *Cooperativity effects in electrocatalytic NO_x reduction*

In the electrocatalytic reduction of NO and/or NO_2^- by Fe(III)-substituted heteropolytungstates, the first step in this process is the formation of a complex with the Fe(II) form of the POM and nitrogen oxide. The actual catalytic step takes place with remarkable enhancement of the current intensity, and it occurs at more negative potentials in the reduction domain where the W(VI) centers accumulate a suitable number of electrons within the complex framework for subsequent delivery. With the goal of saving energy by moving the electron reservoir closer to the Fe(III)-reduction potential, several Wells–Dawson-type POMs were synthesised, including α_1-$P_2(FeOH_2)W_{17}O_{61}^{7-}$ and α_2-$P_2(FeOH_2)Mo_2W_{15}O_{61}^{7-}$ in which the Fe- and W-waves or Fe- and Mo-waves merge in appropriate pH media [14,36]. This strategy turns out to be favorable, and the entire catalytic process shows up at the reduction potential of the Fe(III) center, which is now observed concomitantly with the Mo(VI) or W(VI) reduction waves. The same phenomenon is observed with $M_2Fe_2X_4$ (X = P or As; M = Zn(II) or Mn(II)) [62,99]. The results are illustrated briefly with $Mn_2Fe_2P_4$ in Fig. 23, with $NaNO_2$ as the starting substrate. An important current intensity increase is observed with increasing γ values (γ is the excess parameter defined as $\gamma = C^{\circ}_{NO_x}/C^{\circ}_{POM}$) at the reduction potential of the Fe(III) centers in a pH 1 solution (*vide supra* for the behaviour of $NaNO_2$ in this medium). In this potential domain, no reduction is observed for NO or HNO_2 present in the solution. Fig. 23 shows unambiguously that the catalytic process begins simultaneously with the reduction of the Fe(III) centers. Furthermore, it is worth noting the high efficiency of the electrocatalysis, even though modest γ values were used. Finally, in

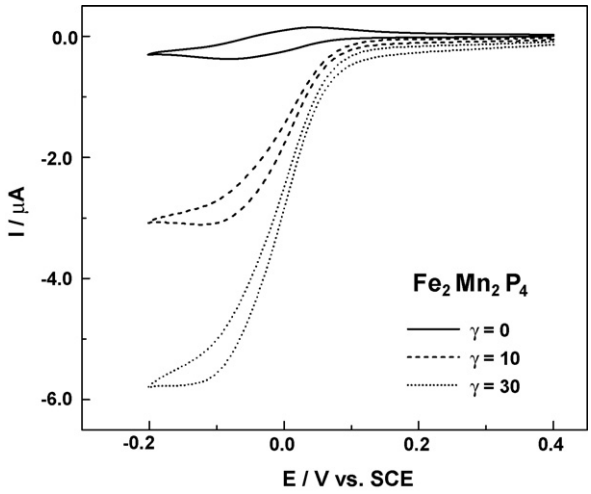

Fig. 23. Cyclic voltammetry study of the electrocatalytic reduction of nitrite with a 2×10^{-4} M solution of $Fe_2Mn_2P_4$ in a pH 1 medium (0.5 M $Na_2SO_4 + H_2SO_4$). The scan rate was 2 mV s^{-1}, the working electrode was glassy carbon, and the reference electrode was SCE (taken from Ref. [99]).

the timescale of cyclic voltammetry, Fe_2P_4 shows the same phenomenon as $Fe_2Mn_2P_4$ concerning the electrocatalytic reduction of NO and NO_2^-. However, the latter complex might be a better choice for this catalytic process due to the improved stability of its Fe(II) forms [98]. Under the same experimental conditions, $Mn_2Fe_2As_4$ also shows good catalytic efficiency for the reduction of nitrite. In addition, its activity at 0 V is 25% higher than that of $Mn_2Fe_2P_4$ due to the positive potential shift of the Fe(III) waves in the former complex compared with the latter due to the different heteroatoms (*i.e.* As *versus* P).

However, in a pH 5 medium, the catalytic process (obtained with $NaNO_2$ as the starting substrate) is no longer observed in the iron-reduction potential domain, but is relegated to the reduction potential of the first W-wave. This observation is in full agreement with the expected absence of NO and HNO_2 in this medium. In contrast, experiments with pure NO [10,39] at pH 5 show that the catalytic process starts directly in the iron reduction potential domain. We have also checked the catalytic reduction of NO at pH 1. All these results converge to designate NO as the species electrocatalytically reduced by the present complexes throughout the pH domain evaluated.

In the foregoing experiments, the electrochemical behaviours of substituent metal cations (Mn(II) or Zn(II)) in the central core of POMs do not exist or are not concerned in the potential domain explored for the catalytic processes. Nonetheless, their presence exerts a beneficial influence on the catalytic reduction of HNO_2 or NO. In summary, there are three features in the preceding results that are favourable for the use of these mixed metal sandwich-type POMs in the electrocatalytic reduction of HNO_2 and NO. First, these POMs are stable from pH 0 to at least 6, a feature not shared by the otherwise efficient molybdic or molybdo-tungstic POMs. Second, these complexes show the enhanced stability of the Fe(II) state within the mixed-metal complexes relative to those observed in their lacunary precursors, Fe_2As_4 and Fe_2P_4. Finally, the third feature exhibited by these complexes which is favourable for electrocatalytic processes is the ability of the Fe-based redox waves to trigger the catalytic processes without any direct interference from the W(VI) centers.

6. Conclusion

Unsubstituted POMs, transition-metal-substituted POMs, mixed addenda POMs and sandwich-type POMs constitute a broad family showing promise for efficient and clean electrocatalytic processes. Reduction and oxidation possibilities exist as well. The rich possibilities opened by POMs might be traced to their robustness and versatility when they are handled in appropriate conditions. One of the aims of the present short focused review is to show the usefulness of POMs in selected electrocatalytic processes. This selection leaves room for a wealth of other possibilities. Another aim is to demonstrate clearly that several parameters must be taken into account in the design and study of these processes. New parameters, in addition of those highlighted here, might emerge because POMs with new atomic compositions, new structures and new reactivities, continue to be synthesised and characterised. However, the stability in aqueous or non aqueous solutions is an absolute prerequisite, which excludes the use of several newly synthesised fragments solely known in the solid state.

Much work remains necessary in many directions: a non exhaustive list includes mechanistic studies, rate constant measurements, preparative scale electrolyses, turnover numbers, scale-up of useful electrocatalytic reactions. There is an increasing number of papers in which the electrocatalytic properties of POMs are illustrated by their activities towards substrates like NO_2^-, NO, BrO_3^-, ClO_3^-, IO_3^-, O_2, H_2O_2, . . ., etc. The challenge, however, is to find new POMs or new POM-based systems to decrease overpotentials which remain high for most reactions and improve the overall kinetics.

Finally, our optimistic prediction is that POMs, owing to their versatility and possibility to accommodate nearly all the atoms of the periodic classification, will become popular to drive selected electrocatalytic processes.

Acknowledgments

We thank all our colleagues and coworkers who have participated in the work on Polyoxometalates. As concerns the synthesis and characterization of some POMs, special thanks are addressed to Dr. R. Contant (Université Paris VI), Professor C.L. Hill, Dr. T.M. Anderson and Professor K. I. Hardcastle (Emory University, Atlanta), Professor U. Kortz (International University of Bremen), Professor M.T. Pope and Dr N. Belai (Georgetown University, Washington), Dr. I.M. Mbomekalle and Dr. Y.W. Lu (Université Paris XI).

Appendix A. Redox *versus* chemical catalysis in the homogeneous catalysis of electrode reactions

The first observations of catalytic phenomena in electrochemistry in the early 1930s were followed by attempts at modeling

the example of hydrogen peroxide reduction in the 1940s. A general framework was expressed, in which electron exchange occurred in solution between the reduced catalyst and the substrate, thus regenerating the catalyst and explaining the observed catalytic effect. In short, electron transfers to or from a molecule must be viewed as a succession of elementary electrochemical and chemical reaction steps. Such simplified reaction schemes served as the basis for theoretical analysis of catalytic phenomena. In molecular electrochemistry, electrochemical reductions can therefore be sketched by the following reaction schemes:

For the catalyst (P):

$$P + 1e \rightleftarrows Q, \quad E^0_{PQ}$$

For the substrate (A):

$$A + 1e \rightleftarrows B, \quad E^0_{AB}$$
$$B \rightarrow C$$

The catalytic effect is reflected in the interaction of Q with A, resulting in the regeneration of P.

$$Q + A \rightleftarrows \ldots \rightleftarrows P + C$$

The only thermodynamic condition then required for this reaction to be driven from left to right is that the standard molar free enthalpy of the reaction be negative, *i.e.* the following inequality must hold: $E^0_{PQ} < E^0_{AC}$, where E^0_{AC} represents the standard redox potential of the A/C couple.

However, this overall scheme might feature two types of successive reaction steps. The first one considers the possibility of solution electron transfers; the second one goes through the formation of an adduct.

The first scheme is simple and reads as follows:

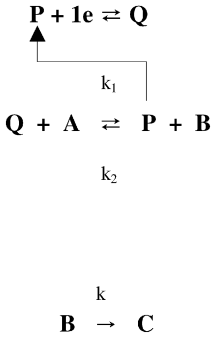

It is worth reminding that the direct reduction of the substrate is realized according to the following pathways:

$$A + 1e \rightleftarrows B, \quad E^0_{AB}$$
$$B \rightarrow C$$

The catalyst constitutes an electron shuttle between the electrode and the solution, where it is engaged in a direct redox electron transfer with the substrate. This type of catalysis is termed *redox catalysis*.

The second reaction scheme reads:

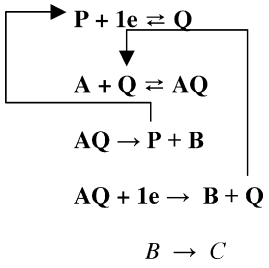

In this case, the reduced form of the catalyst builds up with the substrate a relatively unstable adduct AQ, which then decomposes, eventually after further reduction at the electrode surface or in solution. Finally, either the oxidized form P of the catalyst or its reduced form Q is regenerated. As concerns the substrate, its reduction follows the aforementioned E.C. (electrochemical chemical) mechanism. This type of catalysis is termed chemical catalysis. Finally, it must be pointed out that the clear-cut distinction between redox catalysis and chemical catalysis might be difficult, but amounts ultimately to a detailed study of the nature of the redox reaction.

References

[1] B. Keita, L. Nadjo, Curr. Top. Electrochem. 2 (1993) 77.
[2] C.L. Hill (Guest Ed.) Chem. Rev. 98 (1998) 1–389.
[3] M.T. Pope, Heteropoly and Isopoly Oxometalates, Springer-Verlag, Berlin, 1983.
[4] M.T. Pope, A. Müller (Eds.), Polyoxometalates: From Platonic Solids to Antiretroviral Activity, Kluwer Academic Publications, Dordrecht, 1994.
[5] (a) M.T. Pope, Polyoxo anions: synthesis and structure, in: A.G. Wedd (Ed.), Comprehensive Coordination Chemistry II: Transition Metal Groups 3-6, vol. 4, Elsevier Science, New York, 2004, pp. 635–678 (Chapter 4.10);
(b) R. Contant, G. Hervé, Rev. Inorg. Chem. 22 (2002) 63;
(c) J.J. Cruywagen, Adv. Inorg. Chem. 49 (2000) 127;
(d) J. Berzélius, Pogg. Ann. 6 (369) (1826) 380;
(e) L. Svanberg, H. Struve, J. Prakt. Chem. 44 (257) (1848) 291;
(f) C. Marignac, C. R. Acad. Sci. 55 (1862) 888.
[6] C.L. Hill, Polyoxometalates: reactivity, in: A.G. Wedd (Ed.), Comprehensive Coordination Chemistry II: Transition Metal Groups 3–6, vol. 4, Elsevier Science, New York, 2004, pp. 679–750 (Chapter 4.11).
[7] M. Sadakane, E. Steckhan, Chem. Rev. 98 (1998) 219.
[8] B. Keita, L. Nadjo, Encyclopedia of Electrochemistry, in: A.J. Bard, M. Stratmann (Eds.), Electrochemistry of Polyoxometalates, vol. 7, Wiley-VCH, 2006.
[9] B. Keita, L. Nadjo, Electrocatalysis by chemically modified electrodes of the main inorganic chemicals, Encyclopedia of Electrochemistry, vol. 10, in: A.J. Bard, M. Stratmann (Eds.), Wiley-VCH, in press (no news).
[10] A. Belhouari, B. Keita, L. Nadjo, R. Contant, New J. Chem. 83 (1998).
[11] R. Contant, M. Abbessi, J. Canny, A. Belhouari, B. Keita, L. Nadjo, Inorg. Chem. 36 (1997) 4961.
[12] B. Keita, L. Nadjo, R. Contant, J. Electroanal. Chem. 443 (1998) 168–174.
[13] (a) R. Contant, M. Abbessi, J. Canny, B. Keita, A. Belhouari, L. Nadjo, Eur. J. Inorg. Chem. (2000) 567;
(b) R. Belghiche, R. Contant, Y.W. Lu, B. Keita, M. Abbessi, L. Nadjo, J. Mahuteau, Eur. J. Inorg. Chem. (2002) 1410.
[14] B. Keita, Y.W. Lu, L. Nadjo, R. Contant, M. Abbessi, J. Canny, M. Richet, J. Electroanal. Chem. 477 (1999) 146.
[15] B. Keita, F. Girard, L. Nadjo, R. Contant, J. Canny, M. Richet, J. Electroanal. Chem. 478 (1999) 76–82.
[16] G.A. Tsirlina, V. Yu Kotov, Rossiiskii Khimicheskii Zhurnal 42 (1998) 96–102 (electron transfer kinetics).

[17] I.A. Weinstock, Chem. Rev. 98 (1998) 113–170.
[18] M.T. Pope, Introduction to polyoxometalate chemistry nato science series, II: mathematics, physics and chemistry, Polyoxometalate Mol. Sci. 98 (2003) 3–31.
[19] L.E. Briand, G.T. Baronetti, H.J. Thomas, Appl. Catal. A: Gen. 256 (2003) 37–50.
[20] B. Keita, L. Nadjo, Mater. Chem. Phys. 22 (1989) 77.
[21] L.C. Baker, Plenary Lecture Proceedings XV International Conference on Coordination Chemistry, Moscow, 1973.
[22] W. Kutner, J. Wang, M. L'Her, R.P. Buck, Pure Appl. Chem. 70 (1998) 1301.
[23] B. Keita, Y.W. Lu, L. Nadjo, R. Contant, M. Abbessi, J. Canny, M. Richet, J. Electroanal. Chem. 477 (1999) 146–157.
[24] B. Keita, K. Essaadi, L. Nadjo, M. Desmadril, Chem. Phys. Lett. 237 (1995) 411.
[25] K. Essaadi, B. Keita, L. Nadjo, R. Contant, J. Electroanal. Chem. 367 (1994) 275.
[26] B. Keita, K. Essaadi, L. Nadjo, R. Contant, Y. Justum, J. Electroanal. Chem. 404 (1996) 271.
[27] B. Keita, K. Essaadi, A. Belhouari, L. Nadjo, R. Contant, Y. Justum, C.R. Acad. Sci. Paris, série IIc, 1998, p. 343.
[28] B. Keita, I.M. Mbomekalle, L. Nadjo, P. de Oliveira, A. Ranjbari, R. Contant, C. R. Chim. 8 (2005) 1057.
[29] K. Drauz, H. Waldmann, Enzyme Catalysis on Organic Synthesis—A Comprehensive Handbooks, vol. 2, VCH, Weinheim, 1995.
[30] E. Steckhan, Top. Curr. Chem. 170 (1994) 83.
[31] (a) J.H. Christie, J. Electroanal. Chem. 13 (1967) 79;
(b) J.H. Christie, R.A. Osteryoung, F.C. Anson, J. Electroanal. Chem. 13 (1967) 236;
(c) F.C. Anson, J.H. Christie, R.A. Osteryoung, J. Electroanal. Chem. 13 (1967) 343;
(d) P.J. Lingane, J.H. Christie, J. Electroanal. Chem. 13 (1967) 227.
[32] (a) R.A. Marcus, J. Phys. Chem. 72 (1968) 891;
(b) C.P. Andrieux, C. Blocman, J.M. Dumas-Bouchiat, J.M. Savéant, J. Am. Chem. Soc. 101 (1979) 3431.
[33] J.E. Toth, F.C. Anson, J. Am. Chem. Soc. 111 (1989) 2444–2451.
[34] B. Keita, L. Nadjo, R. Contant, M. Fournier, G. Hervé, (CNRS) French Patent 89/1,728 (1989).
[35] B. Keita, L. Nadjo, R. Contant, M. Fournier, G. Hervé, (CNRS) European Patent Appl. EP 382,644 (1990); Chem Abst. 114 (1991) 191882u.
[36] B. Keita, Y.W. Lu, L. Nadjo, R. Contant, Electrochem. Commun. 2 (2000) 720.
[37] S. Dong, X. Xi, M. Tian, J. Electroanal. Chem. 385 (1995) 227.
[38] X. Xi, S. Dong, J. Mol. Catal. A: Chem. 114 (1996) 257.
[39] B. Keita, A. Belhouari, L. Nadjo, R. Contant, J. Electroanal. Chem. 381 (1995) 243.
[40] J.E. Toth, F.C. Anson, J. Electroanal. Chem. 256 (1988) 361.
[41] L.E. Briand, G.T. Baronetti, H.J. Thomas, Appl. Catal. A: Gen. 256 (2003) 37.
[42] D.P. Smith, M.T. Pope, Inorg. Chem. 12 (1973) 331.
[43] G. Hervé, A. Tézé, M. Leyrie, J. Coord. Chem. 9 (1979) 245.
[44] M.M. Mossoba, C.J. O'Connor, M.T. Pope, E. Sinn, G. Hervé, A. Tézé, J. Am. Chem. Soc. 102 (1980) 6864.
[45] S.P. Harmalker, M.T. Pope, J. Am. Chem. Soc. 103 (1981) 7381.
[46] S.P. Harmalker, M.A. Leparulo, M.T. Pope, J. Am. Chem. Soc. 105 (1983) 4286.
[47] M. Abbessi, R. Contant, R. Thouvenot, G. Hervé, Inorg. Chem. 30 (1991) 1695.
[48] P. Mialane, J. Marrot, E. Rivière, J. Nebout, G. Hervé, Inorg. Chem. 40 (2001) 44.
[49] R. Contant, R. Thouvenot, Can. J. Chem. 69 (1991) 1498.
[50] I.V. Khozevnikov, K.I. Matveev, Appl. Catal. 5 (5) (1983) 135.
[51] H. Ogawa, H. Fujinami, K. Taya, S. Teratani, J. Chem. Soc. Chem. Commun. (1981) 1274.
[52] V.E. Taraban'ko, I.V. Khozevnikov, K.I. Matveev, Kinet. Katal. 19 (1978) 160.
[53] S.F. Davidson, B.E. Mann, P.M. Maitlis, J. Chem. Soc. Dalton Trans. (1984) 1223.
[54] R.G. Finke, B. Rapko, R.J. Saxton, P.J. Domaille, J. Am. Chem. Soc. 108 (1986) 2948.
[55] H. Weiner, R.G. Finke, J. Am. Chem. Soc. 121 (1999) 9831.
[56] K. Nomiya, Y. Nemoto, T. Hasegawa, S. Matsuoka, J. Mol. Catal. A: Chem. 152 (2000) 55.
[57] D.E. Clinton, D.A. Tryk, I.T. Bae, F.L. Urbach, M.R. Antonio, D.A. Scherson, J. Phys. Chem. 100 (1996) 18511.
[58] X. Lopez, C. Bo, J.M. Poblet, J. Am. Chem. Soc. 124 (2002) 12574.
[59] R. Contant, M. Abbessi, R. Thouvenot, G. Hervé, Inorg. Chem. 43 (2004) 3597.
[60] S.P. Harmalker, M.A. Leparulo, M.T. Pope, J. Am. Chem. Soc. 105 (1983) 4286.
[61] S. Zhai, J. Liu, J. Jiang, S. Dong, Electroanalysis 15 (2003) 1165.
[62] I.M. Mbomekallé, R. Cao, K.I. Hardcastle, C.L. Hill, M. Ammam, B. Keita, L. Nadjo, T.M. Anderson, Comptes Rendus 8 (2005) 1077.
[63] B. Keita, I.M. Mbomekalle, P. de Oliveira, A. Ranjbari, Y. Justum, L. Nadjo, D. Pompon, J. Cluster Sci. 17 (2006) 221.
[64] I.M. Mbomekalle, B. Keita, L. Nadjo, R. Contant, N. Belai, M.T. Pope, Inorg. Chim. Acta 342 (2003) 219.
[65] I.M. Mbomekalle, B. Keita, Y.W. Lu, L. Nadjo, R. Contant, N. Belai, M.T. Pope, Eur. J. Inorg. Chem. (2004) 276–285.
[66] H. Han, H. Tachikawa, Front. Biosci. 10 (2005) 931.
[67] S. Fei, J. Chen, S. Yao, G. Deng, D. He, Y. Kuang, Anal. Biochem. 339 (2005) 29.
[68] A. Salimi, R. Hallaj, Talanta 66 (2005) 967.
[69] R.D. Thackrey, T.L. Riechel, J. Electroanal. Chem. 245 (1988) 131.
[70] J.A. Reynaud, B. Maltoy, P. Canessan, J. Electroanal. Chem. 114 (1980) 195.
[71] B. Keita, I.M. Mbomekalle, L. Nadjo, C. Haut, Electrochem. Commun. 6 (2004) 978.
[72] S. Dong, M. Liu, J. Electroanal. Chem. 372 (1994) 95.
[73] T. McCormac, B. Fabre, G. Bidan, J. Electroanal. Chem. 427 (1997) 155.
[74] N.N. Greenwood, A. Earnshaw, Chemistry of the Elements, second ed., Butterworth, Heinemann, 1997, p. 406.
[75] B. Keita, E. Abdeljalil, L. Nadjo, R. Contant, R. Belghiche, Electrochem. Commun. 3 (2001) 56.
[76] B. Keita, E. Abdeljalil, L. Nadjo, B. Avisse, R. Contant, J. Canny, M. Richet, Electrochem. Commun. 2 (2000) 145.
[77] S. Kuwabata, S. Uezumi, K. Tanaka, T. Tanaka, J. Chem. Soc. Chem. Commun. (1986) 135.
[78] S. Kuwabata, S. Uezumi, K. Tanaka, T. Tanaka, Inorg. Chem. 25 (1986) 3018.
[79] I.M. Kolthoff, E.B. Sandell, B. Moskovitz, J. Am. Chem. Soc. 55 (1933) 1454.
[80] T.E. Edmonds, Anal. Chim. Acta 116 (1980) 323.
[81] N.G. Carpenter, D. Pletcher, Anal. Chim. Acta 317 (1995) 287–293.
[82] J. Davis, M.J. Moorcroft, S.J. Wilkins, R.G. Compton, M.F. Cardosi, Analyst 125 (2000) 737–742 (and references therein).
[83] B. Keita, I.M. Mbomekalle, L. Nadjo, R. Contant, Electrochem. Commun. 3 (2001) 267.
[84] B. Keita, I.M. Mbomekalle, L. Nadjo, Electrochem. Commun. 5 (2003) 830.
[85] D. Jabbour, B. Keita, I.M. Mbomekalle, L. Nadjo, U. Kortz, Eur. J. Inorg. Chem. (2004) 2036–2044.
[86] I.R. Epstein, K. Kustin, L.J. Warshaw, J. Am. Chem. Soc. 102 (1980) 3751.
[87] L.-H. Bi, U. Kortz, S. Nellutla, A.C. Stowe, N.S. Dalal, B. Keita, L. Nadjo, Inorg. Chem. 44 (2005) 896–903.
[88] S. Nellutla, J. van Tol, N.S. Dalal, L.H. Bi, U. Kortz, B. Keita, L. Nadjo, G.A. Khitrov, A.G. Marshall, Inorg. Chem. 44 (2005) 9795.
[89] I.M. Mbomekalle, B. Keita, L. Nadjo, P. Berthet, K.I. Hardcastle, C.L. Hill, T.M. Anderson, Inorg. Chem. 42 (2003) 1163.
[90] D. Jabbour, B. Keita, L. Nadjo, U. Kortz, S.S. Mal, Electrochem. Commun. 7 (2005) 841.
[91] B. Keita, M. Benaïssa, L. Nadjo, R. Contant, Electrochem. Commun. 4 (2002) 663.

[92] R. Greef, R. Peat, L.M. Peter, D. Pletcher, J. Robinson, Instrumental Methods in Electrochemistry, Ellis Horwood, England, 1985 (Chapter 6).
[93] A. Hiskia, E. Papaconstantinou, Inorg. Chem. 31 (1992) 163.
[94] (a) D.C. Duncan, C.L. Hill, J. Am. Chem. Soc. 119 (1997) 243;
(b) A.M. Khenkin, L. Weiner, Y. Wang, R. Neumann, J. Am. Chem. Soc. 123 (2001) 8531.
[95] J. Zhang, F.C. Anson, J. Electroanal. Chem. 341 (1992) 323.
[96] N. Alonso-Vante, H. Tributsch, O. Solorza-Feria, Electrochimica Acta 40 (1995) 567.
[97] B. Keita, F. Girard, L. Nadjo, R. Contant, R. Belghiche, M. Abbessi, J. Electroanal. Chem. 508 (2001) 70.
[98] I.M. Mbomekalle, B. Keita, L. Nadjo, W.A. Neiwert, L. Zhang, K.I. Hardcastle, C.L. Hill, T.M. Anderson, Eur. J. Inorg. Chem. (2003) 3924.
[99] B. Keita, I.M. Mbomekalle, Y.W. Lu, L. Nadjo, P. Berthet, T.M. Anderson, C.L. Hill, Eur. J. Inorg. Chem. (2004) 3462.
[100] I.M. Mbomekalle, B. Keita, M. Nierlich, U. Kortz, P. Berthet, L. Nadjo, Inorg. Chem. 42 (2003) 5143.
[101] T.M. Anderson, X. Zhang, K.I. Hardcastle, C.L. Hill, Inorg. Chem. 41 (2002) 2477.